Journal Pre-proof

Development of Ceramic 3D/4D Printing in China

Xinya Lu , Guo Liu , Jian Lu

PII: S2950-4317(24)00048-0
DOI: https://doi.org/10.1016/j.amf.2024.200158
Reference: AMF 200158

To appear in: *Additive Manufacturing Frontiers*

Received date: 20 May 2024
Revised date: 4 July 2024
Accepted date: 8 July 2024

Please cite this article as: Xinya Lu , Guo Liu , Jian Lu , Development of Ceramic 3D/4D Printing in China, *Additive Manufacturing Frontiers* (2024), doi: https://doi.org/10.1016/j.amf.2024.200158

Development of Ceramic 3D/4D Printing in China

Xinya Lu[a, 1], Guo Liu[b,1], Jian Lu[a,c,d,e,*]

[a] Department of Materials Science and Engineering, City University of Hong Kong, Hong Kong, 999077, China.
[b] CAS Key Laboratory of Mechanical Behavior and Design of Materials, Department of Modern Mechanics, University of Science and Technology of China, Hefei, 230027, China.
[c] CityU-Shenzhen Futian Research Institute, Shenzhen, 518045, China.
[d] Hong Kong Branch of National Precious Metals Material Engineering Research Center, City University of Hong Kong, Hong Kong, 999077, China.
[e] Centre for Advanced Structural Materials, City University of Hong Kong Shenzhen Research Institute, Greater Bay Joint Division, Shenyang National Laboratory for Materials Science, Shenzhen, 518057, China.

[1] These authors contributed to this work equally.
[*]Corresponding author. Email: jianlu@cityu.edu.hk(J. Lu)

Abstract

China derives its name from its rich legacy of traditional ceramic arts, which has inspired generations of people in China and beyond to improve their ceramic processing skills. The review categorises the various ceramic additive manufacturing techniques developed in China into dot-by-dot, line-by-line, and area-by-area additive manufacturing techniques, according to their corresponding dimensional printing strategies. These techniques are categorized according to ISO standards, with an overview of representative achievements by Chinese research groups for each method. The review also summarizes and compares materials, printing parameters, and product properties in those studies, highlighting differences in printing speeds among different printing strategies. In addition, milestones in contemporary ceramic four-dimensional (4D) printing are illustrated in terms of the new material (4D printing elastomer-derived ceramics), new process (4D additive–subtractive manufacturing of ceramics), and new function (4D printing shape memory ceramics). Finally, the prospects for ceramic printing and its applications are discussed.

Key words: Additive manufacturing; Ceramic; China; 4D printing; Additive–subtractive manufacturing; Shape memory ceramics

1. Introduction

Additive manufacturing, also referred to as three-dimensional (3D) printing, emerged in the manufacturing sector three decades ago. In the last five years, this innovative manufacturing method has garnered significant attention [1]. It is particularly advantageous for producing complex structures and is well-suited for customised production. Today, a variety of 3D printing technologies, including stereolithography (SLA), selective laser sintering (SLS), fused deposition modelling (FDM), laminated object manufacturing (LOM), binder jetting (BJT), and selective laser melting (SLM), have been developed. The operational principles of these techniques are illustrated in the technology roadmap of additive manufacturing (**Fig. 1**). Ceramics, renowned for their superior thermal, mechanical, electrical, and biocompatible properties, have found widespread applications in various industries [2]. However, conventional ceramic manufacturing processes often require costly moulds or dies that are unsuitable for creating complex structures. Moreover, the inherent brittleness and hardness of most ceramics pose significant challenges for machining [3]. In response, the integration of additive manufacturing into the ceramics industry has been revolutionary, addressing these limitations while introducing new challenges [2].

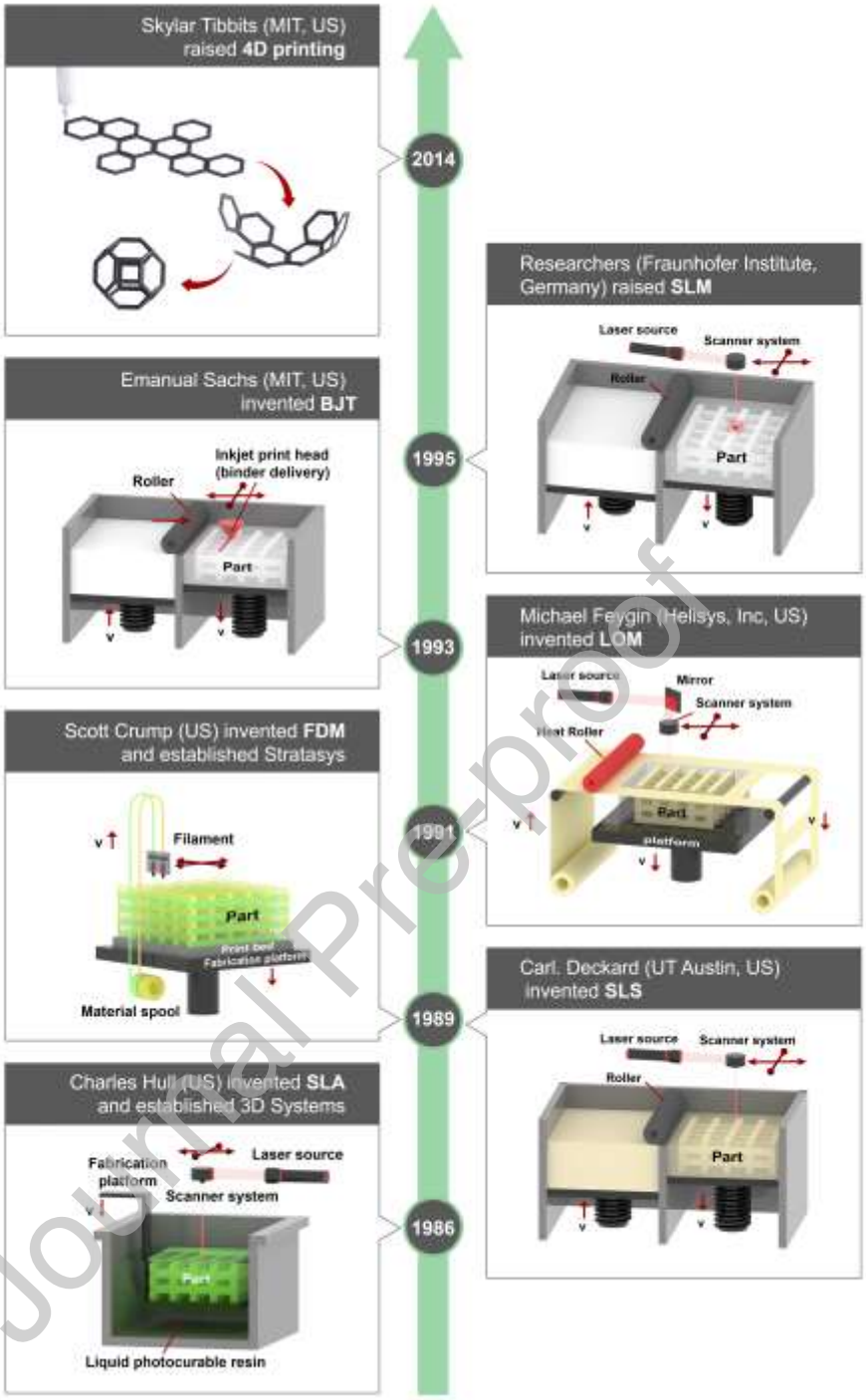

Fig. 1. Technical roadmap of additive manufacturing [1].

In China, additive manufacturing or 3D printing of ceramic materials remains a hot topic during the last five years, and 4D printing of ceramic materials is drawing more and more attention since its birth in 2018. **Fig. 2** illustrates the number of Chinese publications on 3D-printed ceramics over the past decade, along with their relative percentage. These publication counts were extracted

from *Web of Science* using the keywords 'additive manufacturing / 3D printing / 4D printing + ceramic', and the keyword 'address = (China)' was added to filter Chinese publications specifically. Notably, since 2014, the field of ceramic additive manufacturing has experienced rapid growth, with a significant upward trend in contributions from Chinese researchers. This article reviews the development of ceramic printing in China, progressing from 3D to 4D ceramic printing.

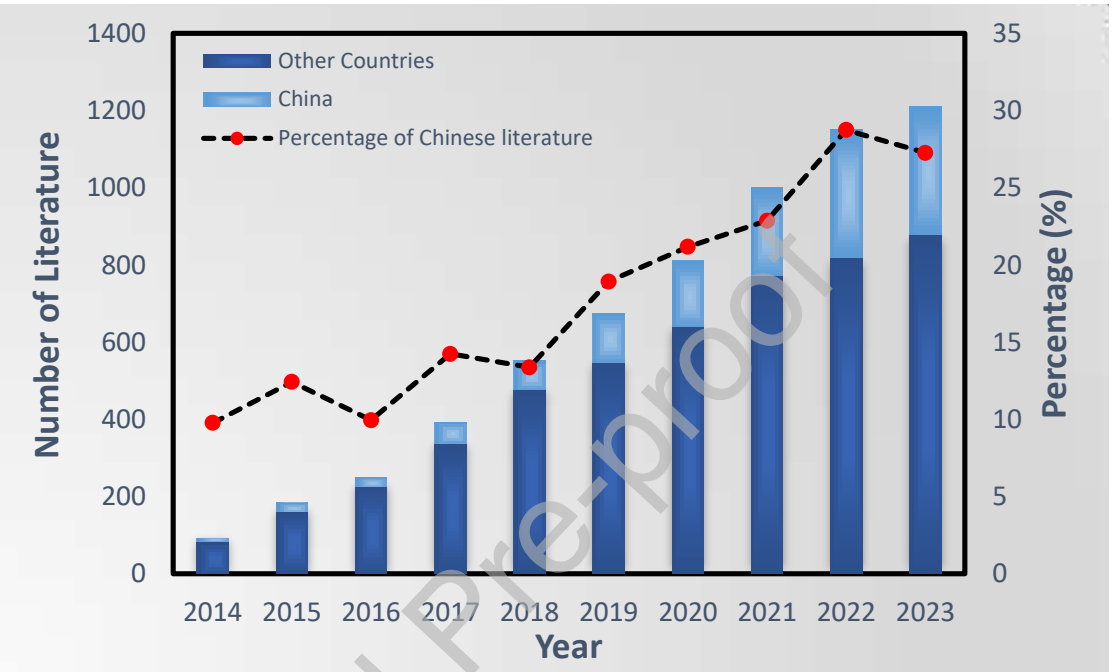

Fig. 2. Number of publications on ceramic additive manufacturing / 3D printing / 4D printing in China annually from 2014 to 2023.

2. Additive Manufacturing of Ceramics

This section reviews the achievements of Chinese research groups in developing various additive manufacturing methods for ceramics. Additive manufacturing techniques are categorised into three classes based on their fabrication mode: dot-by-dot, line-by-line, and layer-by-layer. Table 1 provides an overview of the terminology for additive manufacturing methods as classified by ISO/ASTM 52900:2021, along with the corresponding subdivisions. This paper primarily focuses on the following techniques: MJT, BJT, direct ink writing (DIW), FDM, powder bed fusion (PBF), directed energy deposition (DED), SLA, one-photon micro-stereolithography (OμSL), digital light processing (DLP), and LOM. Compared with these techniques, Chinese groups have conducted limited research on other techniques to date.

Table 1. Terminology for additive manufacturing of ceramics.

Terms following ISO standard	Other terms	Printing dimension
Material jetting (MJT)	Inkjet printing (IJP)	Dot-by-dot
Binder jetting (BJT)	/	
Material extrusion (MEX)	Direct ink writing (DIW)	Line-by-line
	Fused deposition modelling (FDM)	
Powder bed fusion (PBF)	Selective laser sintering (SLS)	
Directed energy deposition (DED)	/	
Vat photopolymerization (VPP)	Stereolithography (SLA)	Area-by-area
	One-photon micro-stereolithography (OμSL)	
	Digital light processing (DLP)	
Sheet lamination (SHL)	Laminated object manufacturing (LOM)	

2.1. Dot-by-dot additive manufacturing

2.1.1 Material jetting (MJT)

Material jetting **(**MJT), also known as IJP, is currently one of the most widely used additive manufacturing techniques. Initially developed as a 2D method for printing documents in the 1960s, it was adapted into a 3D additive manufacturing technique approximately two decades thereafter [4, 5]. MJT generally operates in two modes, i.e., continuous and drop-on-demand [6], the latter of which is commonly favoured for its high resolution and precision [2, 6]. MJT offers exceptional dimension accuracy, although the sizes of printed samples can be affected by the fusion and solidification of droplets [7]. Its other advantages include low cost of manufacturing and equipment and the possibility of multi-material fabrication. However, the range of materials that can be manufactured by MJT is limited compared with other commonly used additive manufacturing methods [4]. MJT has been applied in various fields, including bioengineering, ceramics, conductive circuitry, and optics [8].

Efforts have been made to explore the potential applications of MJT technology in various industries. Chen et al. have made notable advancements in using MJT to manufacture solid oxide fuel cells (SOFCs). In 2018, their research team developed an innovative aqueous-based cathode suspension using La0.6Sr0.4Co0.2Fe0.8O3-δ (LSCF) powders for MJT. The suspension's high dispersity and long-term stability were enhanced through the addition of triethanolamine (TEA) as a dispersant [9]. In the additive manufacturing process of the SOFCs, gadolinia-doped ceria (GDC) was first inkjet-printed onto the electrolyte, and LSCF ink was then printed on top of the GDC. The

deposition spacings of GDC and LSCF inks are 20 μm and 25 μm, respectively [10]. Subsequent investigations focused on post-processing strategies for MJT-fabricated fuel cells, comparing the power densities of different SOFC samples dried above and below room temperature and sintered at temperatures ranging from 850 °C to 1050 °C. The results revealed that cells dried in a furnace and sintered at 900 °C exhibited the highest power density and optimal mechanical strength [11]. MJT has also been applied to produce other electronic components, such as circuits-on-ceramics structures. For example, Huang et al. successfully manufactured an LED circuit using reduced graphene oxide (rGO) printed on an alumina ceramics substrate. The MJT-fabricated Al_2O_3 ceramics achieved a maximum power density of 95.2% at a sintering temperature of 1600 °C, and the conductivity of the overall circuits-on-ceramics structure was $5.34 \times 10^2\ S \cdot m^{-1}$ [12]. Moreover, MJT is compatible with bioceramics such as hydroxyapatite (HA) in the form of air-jet-milled powders or spherical powders [13] and calcium phosphate, which can be biodegraded at a tailored rate for personalised skull bone tissue reconstruction [14].

As a widely utilised additive manufacturing technology, MJT eliminates the need for conventional and costly moulding processes, offering enhanced flexibility and quality in industrial fabrication. Recently, Liang et al. pioneered the use of MJT in producing low-temperature co-fired ceramics (LTCCs), commonly used as substrates in microwave technology. The research group developed a stable SiO_2-H_3BO_3 nanoceramic ink. The fabricated samples demonstrated an ultra-low dielectric constant and exhibited excellent stability under high temperatures and frequencies. Furthermore, the same research group successfully fabricated a university badge from LTCC ink, with a surface resolution of 60 μm [15]. In a further study, it was discovered that a solid content of 35% optimised the ink printability. LTCCs have demonstrated extraordinary thermal and dielectric properties [16]. Zhong et al. leveraged the capabilities of NanoParticle Jetting (NPJ) to fabricate dense zirconia ceramic parts with highly detailed components and customisable mechanical properties (**Fig. 3(d)**). The surface roughness of the samples measured less than 0.33 μm, and their fracture toughness reached up to 7.52 MPa $m^{1/2}$ [17].

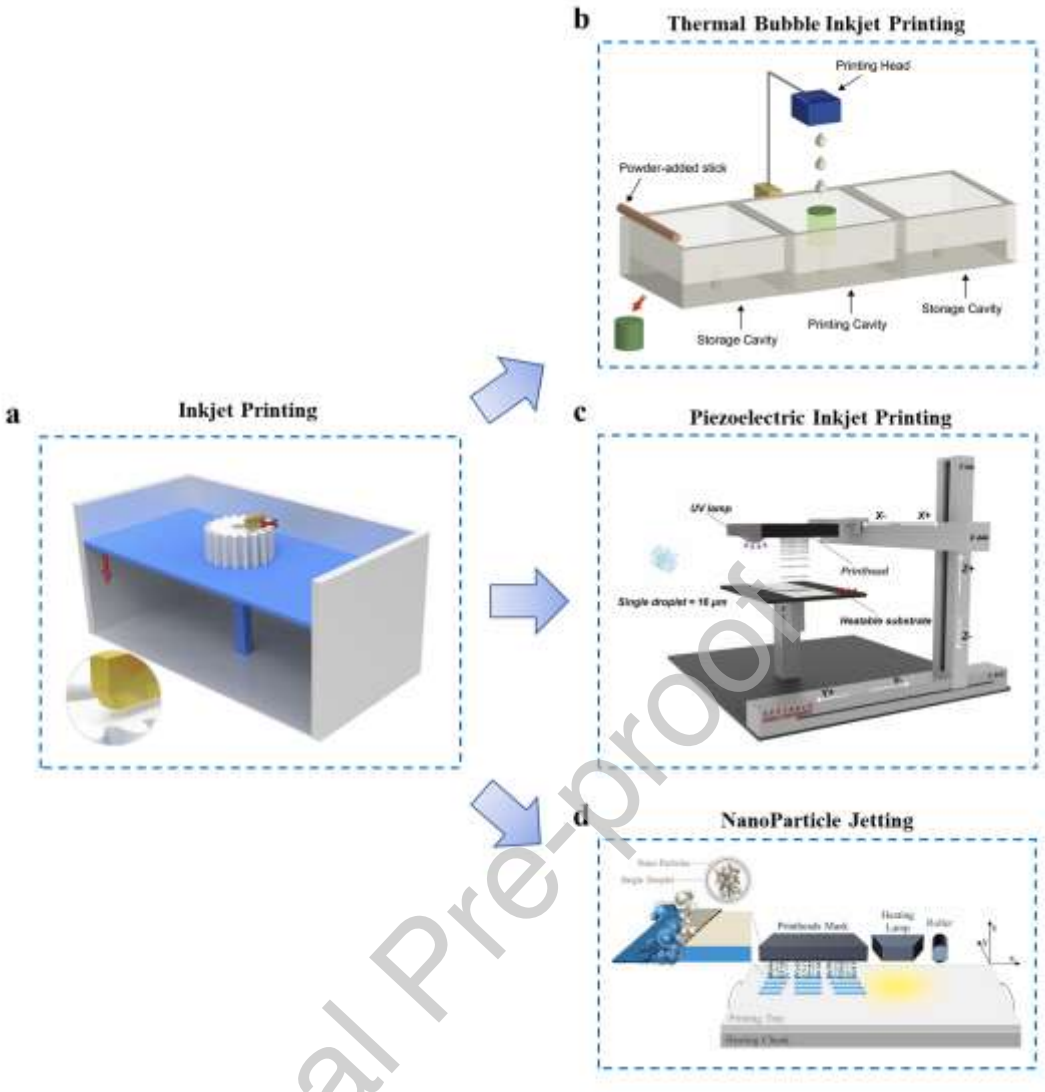

Fig. 3. Illustrations of MJT manufacturing processes: (a) Schematic of MJT [2]; (b) Thermal bubble MJT [12]; (c) Piezoelectric MJT, illustrated by a five-axis inkjet device developed by Liang et al. [15]; (d) NPJ printing [17].

2.1.2 Binder jetting (BJT)

Compared to MJT where materials were directly jetted from the printhead, binder jetting **(**BJT) employs a liquid binder to bond material particles in the powder bed. This process, utilising multiple printheads, combines high efficiency with low cost [18]. BJT offers a higher solid loading than MJT, with no need for supporting structures. However, it is difficult to introduce additives into the BJT process, and post-processing can be expensive [4]. Taking advantage of the high forming efficiency of BJT and the avoidance of thermal deformation, Feng et al. developed silicon carbide ceramics through BJT and subsequent post-processes (**Fig. 4(b)**). First, the SiC green body was 3D-printed

via BJT. Phenolic resin impregnation and pyrolysis (PRIP) was then conducted to increase the carbon density and reduce porosity, followed by liquid silicon infiltration (LSI). The final product exhibited superior wear resistance and a significant increase in flexural strength, from 7.7 MPa to 257 MPa, compared with the initial SiC green body. This additive manufacturing process has been validated for parts with complex geometries, such as turbine discs [19]. In a separate study, the same research group extensively investigated BJT-printed alumina-based ceramics and revealed that alumina-based ceramic functionally graded materials could be toughened through co-sintering with 316L stainless steel [20]. Sintering additives such as zirconium basic carbonate (ZBC) [21] and $Ca(OH)_2-MgO-SiO_2$ [22] were proven feasible to enhance the mechanical strength and other properties of alumina samples fabricated by BJT. There were also efforts made on introducing nanoparticle additives to BJT process [23, 24]. Furthermore, doping has been identified as an effective method for enhancing the strength of pure alumina ceramics. The research group found that alumina doped with 4 wt.% $Ti.O_2$ and 1 wt.% CuO and sintered from 1300 °C to 1400 °C exhibited an optimal flexural strength of approximately 27.44 MPa, 86.8% higher than that of pure alumina ceramics [25].

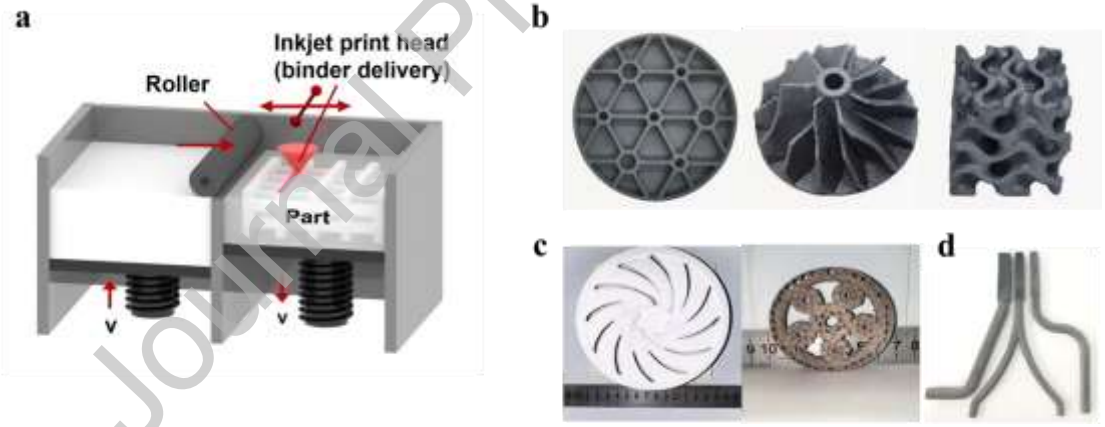

Fig. 4. BJT manufacturing of complex structural ceramic parts: (a) Schematic of BJT [1]; (b) Si–SiC parts: optical mirror, turbine disc, and topology of gyroid structure [19]; (c) Unconventional alumina ceramic gears [25]; (d) Complex-shaped alumina ceramic cores [21].

2.2. Line-by-line additive manufacturing

2.2.1 Material extrusion (MEX)

2.2.1.1 Direct ink writing (DIW)

As one of the most simple and versatile MEX additive manufacturing techniques, DIW is characterised by its low cost, technical simplicity, and broad range of ink compatibility [26], including colloidal inks, nanoparticle-filled inks, sol–gel inks, and others [4]. In the printing process, inks are extruded as a continuous filament through a nozzle, constructing the 3D object in a line-by-line, layer-by-layer manner. The rheological properties of the inks are curial, and with appropriate viscosity they can flow smoothly through the nozzle while retaining their shapes after deposition [4, 5]. DIW therefore has less stringent requirements for supporting structures than other additive manufacturing methods, such as PBF and vat polymerization (VPP) [2]. DIW is capable of fabricating materials with exceptional properties, and ceramic DIW holds significant potential in the aerospace, automotive, biomedicine, energy, and other sectors [27].

Due to its broad ink compatibility, DIW allows for the preparation of slurries with various compositions and additives for the fabrication of complex products, enabling controllable microstructures with tailored properties. Recently, Yang et al. developed silicon nitride aqueous suspensions with customised rheological properties, resulting in dense Si_3N_4 ceramics with enhanced strength. The flexural strength of DIW-printed silicon nitride reached 348 MPa with a 40 vol% suspension [28]. In a related study, the extrusion mechanics of Si_3N_4 inks under pneumatic pressure were examined, enabling the 3D printing of ceramic structures with programmable microchannels formed between the filaments [29] (**Fig. 5(f)**). Furthermore, the same research team comprehensively investigated the rheological relationship between Si_3N_4 inks and carboxymethyl cellulose hydrogels for printing large-scale components. A large, thin-walled cone was successfully fabricated by DIW, exhibiting no defects or deformations during the debinding and sintering processes [30]. Concurrently, Zhang et al. focused on developing ceramic foams through DIW, including boehmite gel and ceria (CeO_2) foams, both yielding porous structures with high mechanical strengths [31, 32]. Other ceramic inks compatible with DIW technology include silicon oxycarbide [33], alumina [34, 35], silicon carbide [36], and cordierite ($2MgO \cdot 2Al_2O_3 \cdot 5SiO_2$) particle inks [37], demonstrating the wide application spectrum of this technique.

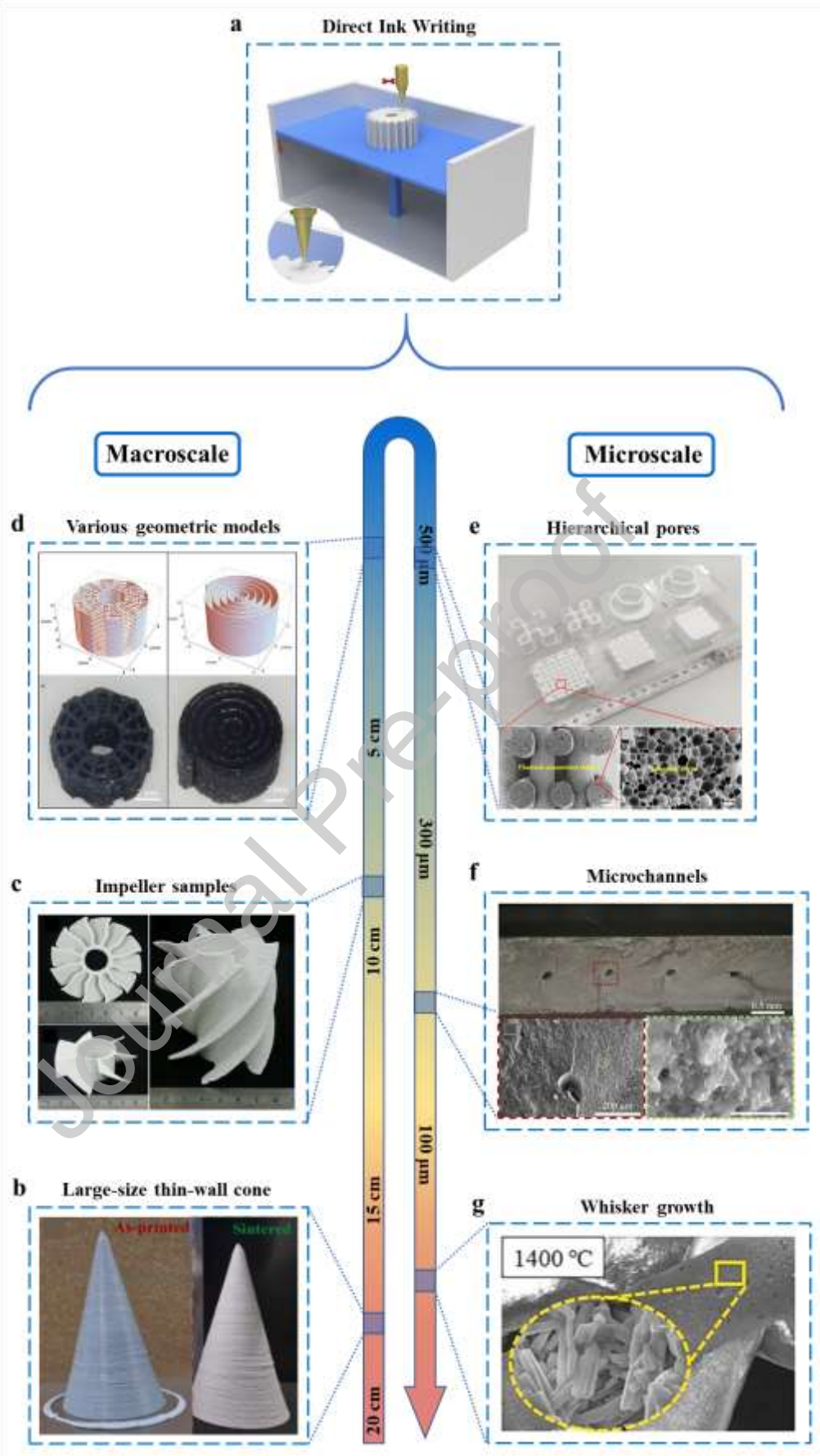

Fig. 5. Complicated DIW-printed structures from macroscale to microscale: (a) Schematic of DIW

[2]; (b) A large-sized thin-walled cone made from silicon nitride (Scale: ~18 cm) [30]; (c) Alumina impeller samples with inclined surfaces (Scale: ~8 cm) [35]; (d) DIW-printed SiC concentric cylindrical structure and multi-layered Archimedean spiral (Scale: ~0.4 cm) [36]; (e) Boehmite gel foams with hierarchical pore structure (Porous filament scale: ~500 μm) [31]; (f) Silicon nitride microchannels (Scale: ~200 μm) [29]; (g) Aluminium borate whiskers (Scale: ~10 μm) [38].

The DIW of ceramics is extensively applied across various manufacturing processes. A notable example is the additive manufacturing of catalyst carriers featuring hierarchical pore structures. Huo et al. proposed a novel method for creating alumina catalyst carriers with a biomimetic vein structure, featuring exceptional mechanical strength and a high specific surface area [39]. Similarly, Lao et al. combined DIW with the in situ growth of whiskers to effectively create both macro- and micron-sized pores in aluminium borate porous ceramics (ABPCs) [38]. Beyond the manufacturing of catalysts, the potential use of DIW techniques extends to the manufacturing of bioimplants such as HA [40], multilevel porous calcium phosphate bioceramic [41], and 4D printing of hybrid ceramic precursor/ceramic materials (**Fig. 6(a)**) [42].

DIW enables the printing of materials with unique properties. For example, Zhu et al. utilised DIW to print a high-strength aligned SiC nanowire skeleton, enhancing the structural integrity of SiC porous ceramics synthesised via chemical vapour infiltration. This innovation led to an increase in compressive strength to 390 MPa [43]. Similarly, Xiong et al. fabricated SiC_w/SiC_p-reinforced 3D porous SiC with a tensile strength of 21.3 MPa [44]. Regarding optical performance, Ji et al. pioneered the fabrication of transparent aluminium oxynitride (AlON) ceramics from water-based ceramic slurries via DIW. The AlON ceramics exhibited optimised mechanical properties and an in-line transmittance of 81.90% at a wavelength of 780 nm [45, 46]. In addition to visible light-transparent ceramics, infrared-transparent ceramics made from 3 mol% yttria-stabilised tetragonal zirconia (3Y-TZP) have also been prepared by DIW [47]. Additionally, DIW has proven to be an effective method for reducing costs and simplifying the manufacturing processes of piezoelectric ceramics. DIW can also be combined with piezo-photocatalytic dye degradation to mitigate secondary pollution in the catalytic process [48]. As illustrated in **Fig. 6(c)**, complex structures of 3D scaffold parts made from lead zirconate titanate (PZT) ink can be printed, offering high flexibility and the possibility for geometric modifications through secondary shaping [49]. In addition, DIW offers flexible solutions for the preparation of elastomeric precursors in developing ceramic 4D printing [50-52], which is introduced in detail in Chapter 3, ‘Ceramic 4D Printing’.

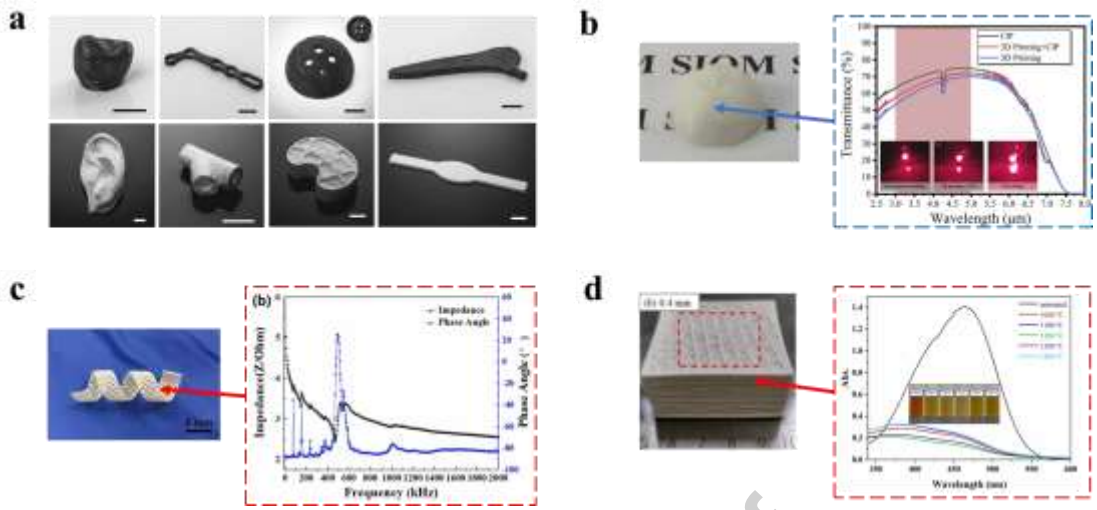

Fig. 6. Application of DIW in various domains: (a) Bioimplants, scale bars: 1 cm [42]; (b) Infrared-transparent 3Y-TZP ceramic dome [47]; (c) Piezoelectric ceramic (PZT) parts with a twisted spiral structure [49]; (d) Photocatalytic activity of ABPCs [38].

2.2.1.2 Fused deposition modelling (FDM)

FDM is another commonly used MEX additive manufacturing methods. In contrast to DIW, which uses inks with the desired rheological properties, FDM employs a preheating chamber to melt the material and thus ensure a smooth extrusion flow. In FDM, 3D printing objects are created through the deposition of melted filaments layer by layer. This method is known for its simplicity, flexible unit size, and cost-effectiveness in terms of materials and equipment, although the product may suffer from compromised strength between layers owing to the staircase effect [2]. As one of the most commonly used additive manufacturing methods, FDM can be applied to fabricate complicated structures at various scales, as shown in **Fig. 7**. Fuzzy logic analysis can be combined with FDM to predict sample properties before manufacturing, which greatly simplifies the process of manufacturing products with tailored properties [53]. Complicated ceramic structures such as turbine rotors and swirl fans can be fabricated by FDM, without the concerns about ultraviolet light scattering that affect the widely used VPP methods [54].

Efforts have been made to broaden the material range and improve the printing effectiveness of FDM, including novel equipment design, product analysis, and ink modification. In 2020, He et al. introduced a screw extrusion system tailored for FDM to handle high solid-loaded granular feedstocks such as alumina and silicon carbide powders. Through the precise control of the screw

speed, nozzle size, and printing temperature, a consistent and programmable extrusion flow was maintained. Zirconia samples produced through this method achieved a post-sintering density of 99% of the theoretical value [55]. Moreover, Shen et al. comprehensively investigated the FDM of zirconia ceramics with intricate geometries using ceramic–polymer granulate feedstock. The microstructure and printing steps were meticulously analysed. The layer thickness of the printed fish model measured 202 μm, closely matching the deposition layer thickness. An interval distance of 30 μm, attributed to stage movement errors in the *x*-direction, was observed. Despite challenges with eliminating pores at junctions, the team successfully produced dense zirconia ceramics with smooth surfaces and uniform structures [56]. Additionally, the research group addressed the challenges associated with the use of preceramic polymers in FDM by incorporating a small amount of thermoplastic polymer to enhance the precursor formability. In these experiments, ≤5 wt.% polypropylene was added to polycarbosilane, resulting in SiC ceramic filaments with a tensile strength of ~471 MPa [57].

FDM is compatible with bioceramics such as HA and is commonly used to print scaffolds from ceramics combined with binders [58]. Zhang et al. successfully fabricated a polylactic acid/HA composite with a nano-HA content as high as 50%. The composite was proven to have reliable printability and printing accuracy with high compressive strength, demonstrating the feasibility of applying FDM in biomedical fields [59]. Furthermore, Wang et al. fabricated a biomimetic scaffold made from piezoelectric whitlockite via FDM, exhibiting a superior repairing effect in a rat calvarial defect compared with a scaffold made of β-TCP [60, 61], which is one of the most commonly used bioceramics for bone substitutes [61].

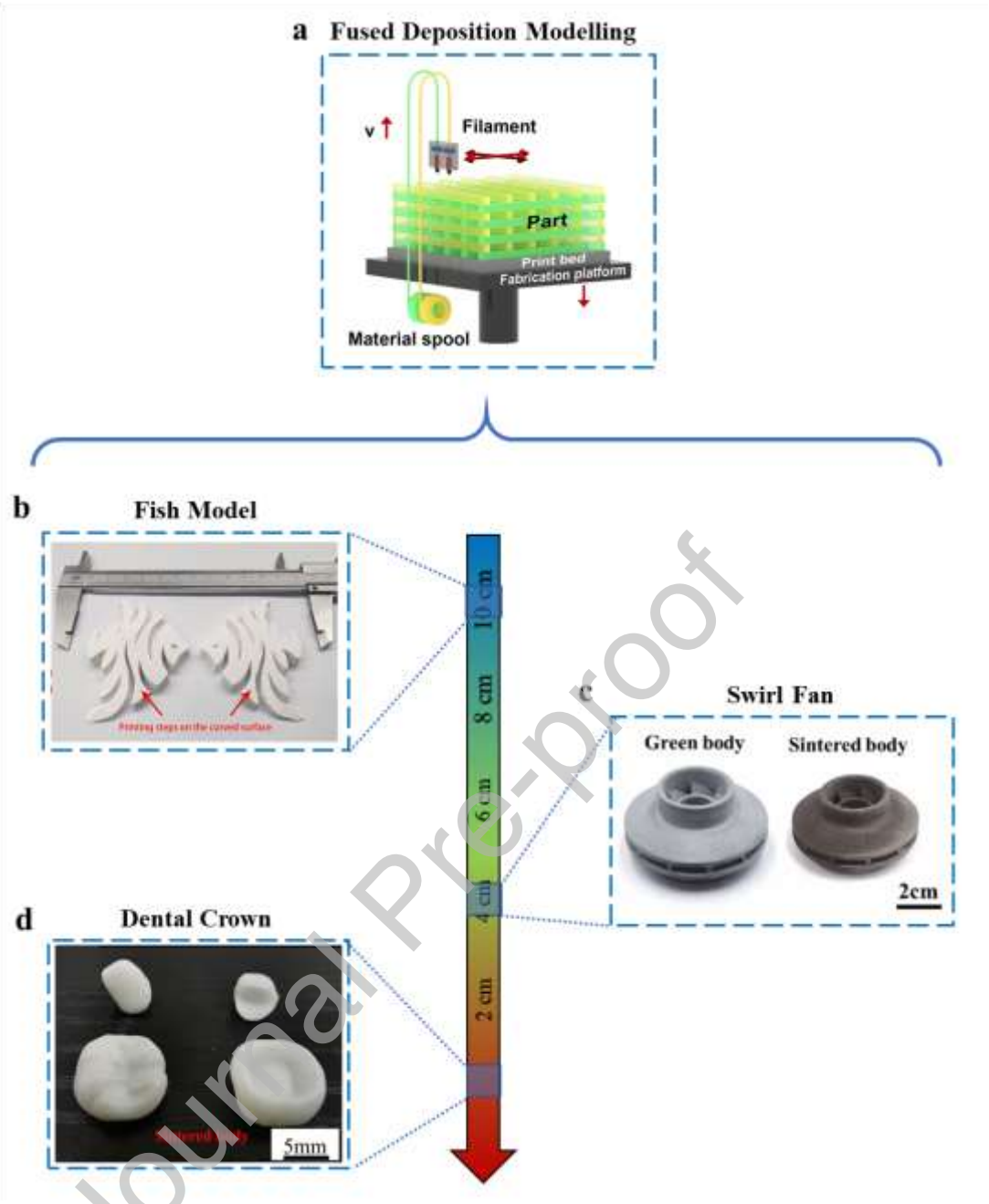

Fig. 7. Complicated ceramic structures fabricated via FDM, with scales ranging from decimetres to millimetres: (a) Schematic of FDM [1]; (b) Zirconia fish models showing printed steps on a curved surface (Scale: ~10 cm) [56]; (c) Silicon nitride swirl fan (Scale: ~4 cm) [54]; (d) Zirconia dental crowns (Scale: ~0.5 cm) [55].

2.2.2 Powder bed fusion (PBF)

PBF was one of the first commercialised additive manufacturing technologies. It has been widely applied to materials such as metals and polymers, although its application to ceramics largely

remains limited to moulds in the aerospace industry (**Figs. 8 (b, e)**) [62, 63] and porous catalyst carriers (**Fig. 8(c)**) [64]. PBF employs one or more heat sources, predominantly laser sources, to induce fusion between powder particles. The drawbacks of PBF primarily include lower accuracy than liquid-based additive manufacturing methods and longer lead times due to the necessary preheating and cooling cycles [4].

Recently, Huo et al. employed PBF to manufacture alumina ceramic catalyst carriers with high specific surface areas. These carriers featured intentionally designed hierarchical pores ranging from microns to nanoscales. The carriers exhibited a specific surface area of 56.324 m^2/g and a porosity of 72.88% [65]. By optimising solidification parameters, Liu et al. 3D-printed Al_2O_3/ZrO_2 eutectic samples with minimised defects. The resulting specimen featured a hardness of 16.7 GPa and a fracture toughness of 4.5 $MPa \cdot m^{1/2}$ [66]. Additionally, Shen et al. successfully fabricated Al_2O_3 / $GdAlO_3$ / ZrO_2 eutectic ceramics with ultra-fine eutectic microstructures, marking a breakthrough in the manufacturing of large-sized complicated structures in a single-step process [67].

Ceramic lattice structures with improved mechanical strength can be produced using PBF. Notably, Wu et al. combined PBF with liquid silicon infiltration processes to fabricate Gyroid-type triply periodic minimal surface structures in SiC ceramics. This novel method significantly increased the elastic modulus of the samples from a modest 121.9 MPa to an impressive 932.0 MPa [68]. Furthermore, the mechanical properties of SiC ceramic matrices can be further enhanced through the integration of carbon fibre reinforcement or the incorporation of carbon black into the SiC powder used in PBF [69, 70].

SLS, a commonly used category of PBF, employs a high-energy laser to selectively sinter ceramic inks. Wu et al. developed moisture–thermal stable alumina-based ceramics for application in solar-driven interface evaporation technology. Their salt-resistant ‘I-shaped’ evaporator, fabricated using SLS, demonstrated stable and superior efficiency in seawater desalination [71]. Additionally, ceramic foams with high porosity, complex structures, and enhanced mechanical properties can be fabricated by SLS [72, 73].

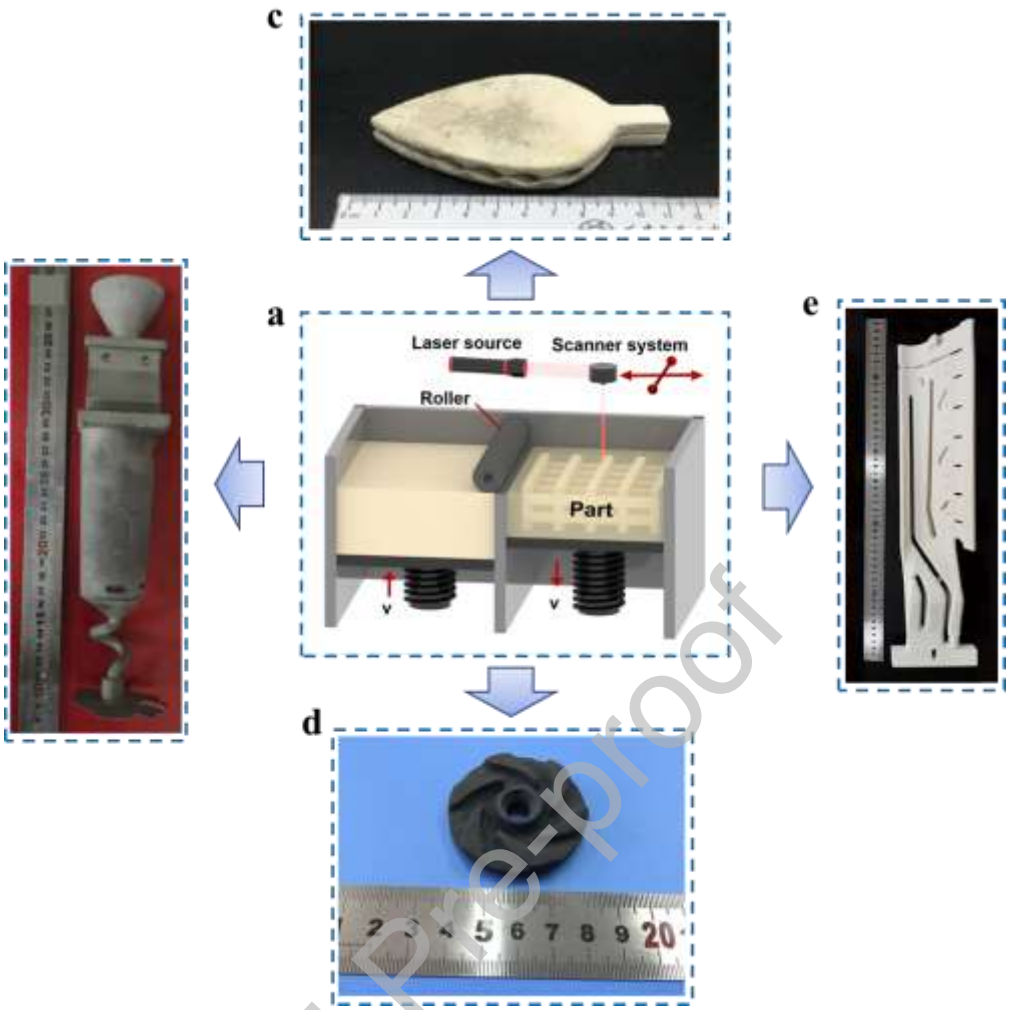

Fig. 8. Applications of PBF-printed ceramics: (a) Schematic of SLS, a common subdivision of PBF [1]; (b) Alumina-based ceramic mould with integral core and shell [62]; (c) Alumina catalyst carriers with bionic leaf vein structures [64]; (d) SiC impeller parts [70]; (e) Silica-based ceramic cores [63].

2.2.3 Directed energy deposition (DED)

In DED additive manufacturing, energy (in the form of a laser or electron beam) is directed to a narrow and focused area of the substrate, where materials are deposited and melt simultaneously. DED offers the capability of producing dense parts with unparalleled control of microstructural features and is particularly suited for repair work and thin layer deposition. However, most DED methods suffer from a poor resolution and surface finish [4].

Laser DED has significant potential in the fabrication of alumina-based eutectic ceramics with a large scale and complicated geometries [74]. Yan et al. conducted a comprehensive investigation of the pores formed on $Al_2O_3-ZrO_2$ eutectic ceramics during laser DED manufacturing. It was

discovered that the pores could be classified into gas holes and shrinkage cavities, and the laser power setting had the greatest influence on pore formation. The same group further devised an ultrasound-assisted direct laser deposition method, resulting in extraordinarily high density and minimised porosity [75]. In a related study, Wu et al. introduced TiCp particles into $Al_2O_3-ZrO_2$ eutectic ceramics with the aim of enhancing their mechanical properties. It was found that 50 wt% TiCp led to the optimal flexural strength and fracture toughness, while 30 wt% TiCp doping resulted in the greatest compressive strength [76]. Additionally, the same group compared the performances of different $Al_2O_3-ZrO_2$ functionally graded ceramics and discovered that 20–25 wt% ZrO_2 could ensure a smooth compositional transition [77]. Elsewhere, Liu et al. conducted comprehensive investigations of an $Al_2O_3/GdAlO_3/ZrO_2$ eutectic ceramic fabricated by laser DED, including its microstructural evolution [74] and the effects of heat treatment on its microstructure [78], surface topology, and mechanical properties [79].

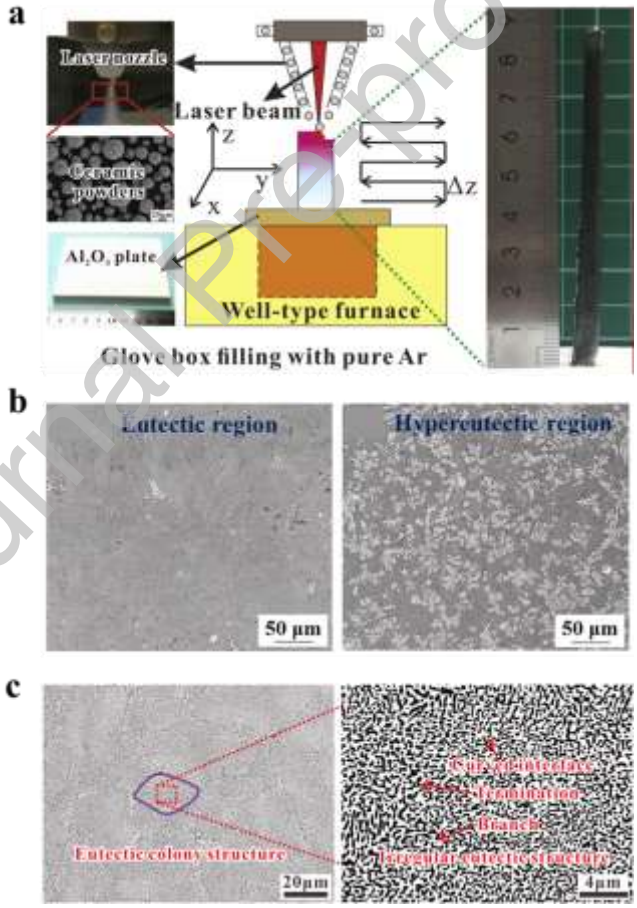

Fig. 9. DED of eutectic ceramics: (a) Schematic of a laser DED printing process [78]; (b) Eutectic and hypereutectic regions of $Al_2O_3-ZrO_2$ functionally graded ceramics [77]; (c) Eutectic colony structure of $Al_2O_3/GdAlO_3/ZrO_2$ [79].

2.2.4 VPP – stereolithography (SLA)

As one of the most prominent VPP 3D printing techniques, SLA 3D printing involves the use of ultraviolet (UV) lasers to cure vats of liquid photopolymer resin, enabling the preparation of conventional ceramic materials with high precision, high surface quality and resolution, and complex geometries compared with MEX. However, excess lateral curing area due to light scattering is a major consideration during SLA 3D printing[2]. Ceramics fabricated by SLA can be applied in many fields, such as ceramic cores for hollow engine blades [80] and bioceramic scaffolds in bone tissue engineering [81, 82].

In 2020, Zhang et al. investigated the impact of additives on SLA 3D-printed alumina ceramics. The incorporation of sintering additives TiO_2 and MgO increased the photosensitivity of the ink slurry, and a flexural strength of ~178.84 MPa was achieved. [83]. The research group also successfully fabricated complex porous SiC architectures, including pyramid and hollowed basket structures (**Fig. 10(a)**). The mechanical strength and density of these ceramics were enhanced through post-process precursor infiltration and pyrolysis [84]. Additives can be employed in SLA not only to endow the product with enhanced or novel characteristics but also to improve the ink printability and fabrication precision. For instance, Chen et al. improved the curability of SiC by introducing diamond powders into the light-curing slurry, resulting in SiC-based composites with strengths of up to ~460 MPa [85]. More recently, Xiao et al. enhanced the printability of lunar regolith simulant paste by adding the copolymer Disperbyk-111. Optimal printing outcomes were achieved with a layer thickness of 50 μm and a placement angle of 0°. The obtained flexural and compressive strengths were 132.21 MPa and 444.23 MPa, respectively [86].

Efforts have also been made to optimise the SLA technique and address the inherent deficiencies associated with specific ceramic inks. Qian et al. examined the light-scattering properties of ceramic particles, which can lead to non-uniform curing during the SLA process. They discovered that the scattering degree of coarse SiO_2 particles could be mitigated through the incorporation of carbon powder into the suspension [87]. Wang et al. investigated the curing mechanisms of SiC-based inks, optimising both the ink composition and printing parameters. The SiC powders were oxidised at 1180°C for 1 h and subsequently hydroxylated with a 0.6 mol/L solution of H_2O_2. The resulting ceramics exhibited excellent mechanical properties and surface quality, demonstrating a flexural strength of 229 MPa [88]. Additionally, the research group successfully fabricated diatomite ceramics characterised by hierarchical pores and high apparent porosity through SLA [89]. Zhang et al. fabricated alumina triply periodic minimal surface (TPMS) structures via SLA (**Fig. 10(c)**), and demonstrated that graded ceramic structures exhibited

significant increase of energy absorption and comparable fracture strength compared to the non-graded structures of similar density, providing a guideline for the design of porous ceramics with pseudo-ductile fracture behaviour [90].

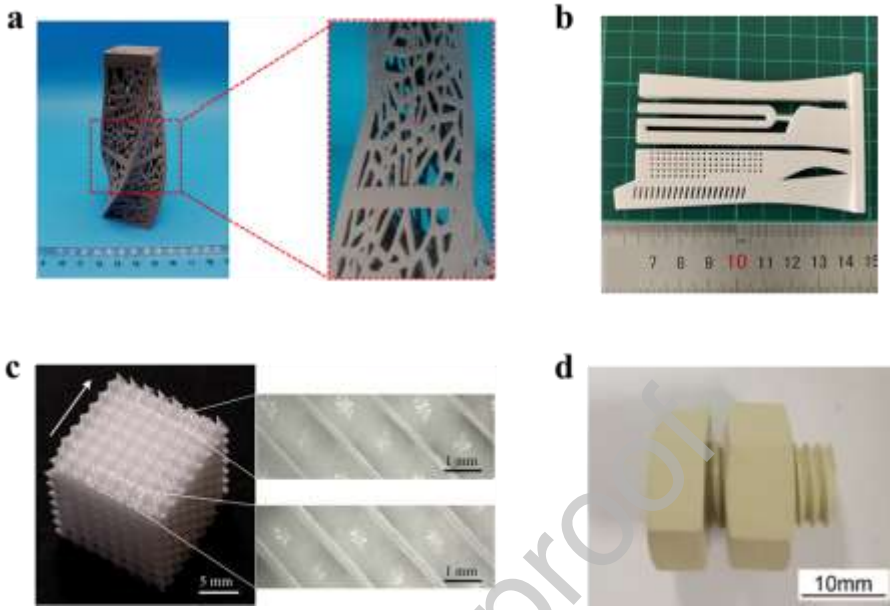

Fig. 10. Complicated ceramic structures printed through SLA: (a) SiC hollow basket [84]; (b) Sintered alumina ceramic core [80]; (c) Graded alumina TPMS structures with pseudo-ductile fracture behaviour [90]; (d) SiC screw and nut [85].

Ceramics with enhanced and tailored properties can be fabricated by SLA. In 2016, Wu et al. reported an innovative approach for preparing zirconia-toughened alumina ceramics based on SLA. The grain of zirconia was 0.35 μm on average, which enhanced the distribution of zirconia along the alumina grain boundaries. The sintered samples exhibited outstanding mechanical properties, with a Vickers hardness of 17.76 GPa, bending strength of 530.25 MPa, and fracture toughness of 5.72 MPa $m^{1/2}$ [91]. In a related study, Zhao et al. examined the creep behaviour and effects of additives on silica ceramics produced via SLA and found that the addition of 15% $ZrSiO_4$ led to a peak creep rate in the specimens [92]. Additionally, Dong et al. investigated the defect distribution and orientation characteristics of fibre-reinforced fused silica (SiO_{2f}/SiO_2) composites and compared the mechanical properties of fused silica composites with varied fibre contents. Parts without cracking or deformation were successfully fabricated by SLA, as displayed in **Fig. 11(a)** [93]. Besides, Wang et al. combined SLA with a hot isostatic pressing process to create magnesium aluminate spinel transparent ceramics and achieved a transmittance of 97%, which approached the theoretical limit [94]. SLA has also proven effective in fabricating piezoelectric ceramics, such as PZT [95].

Recently, K. Zhang et al. utilised SLA to produce ZrO_2 and Al_2O_3 ceramic metamaterials with tailored thermal properties. The thermal expansion coefficients of the 3D quadrangular pyramid (QP) structures were successfully engineered to be negative, zero, and positive, as demonstrated in **Fig. 11(d)** [96].

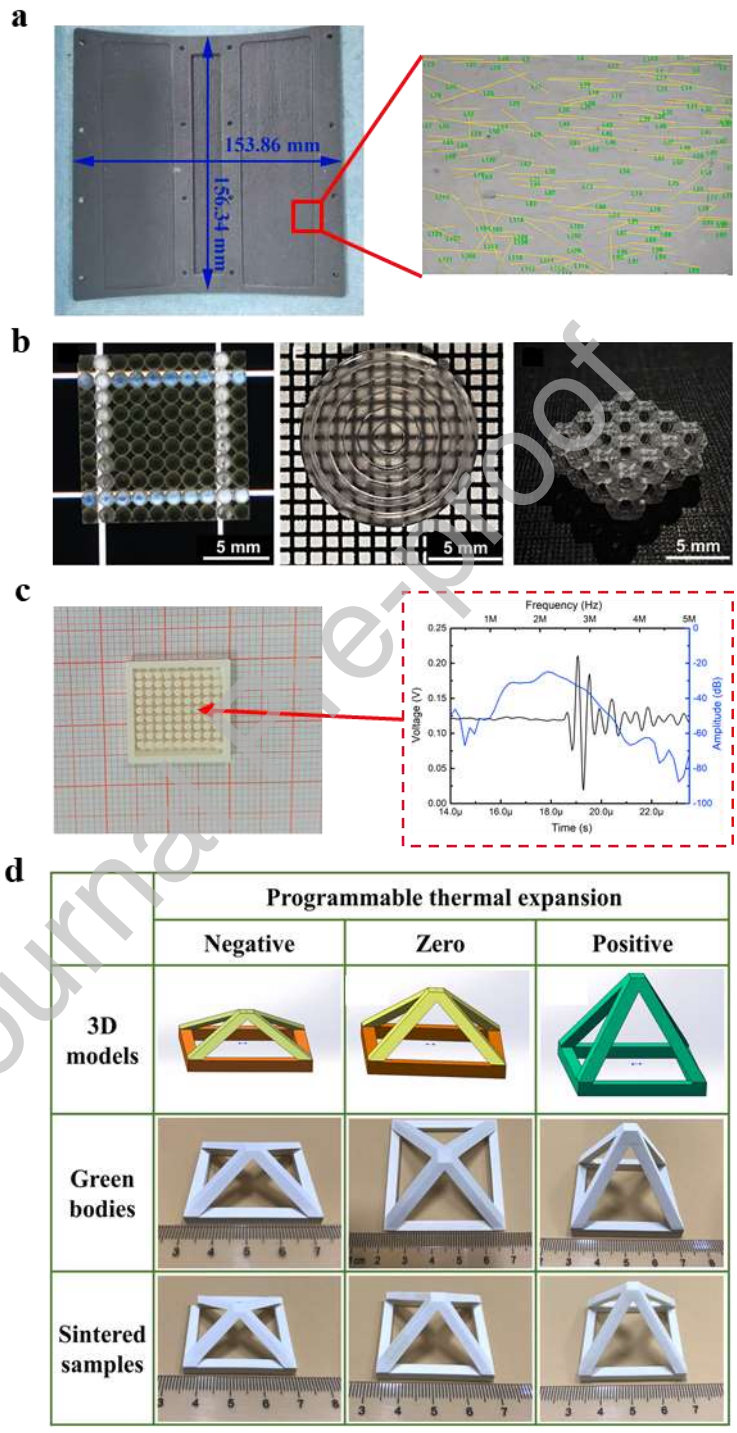

Fig. 11. SLA-printed samples with tailored properties: (a) SLA-printed cambered structural parts made from fibre-reinforced fused silica composites with a 4 wt.% fibre content [93]; (b) Lens and lattice made from transparent spinel ceramics [94]; (c) SLA-printed PZT ceramic array [95]; (d) QP

structures with programmable thermal expansion [96].

2.3. Area-by-area additive manufacturing

2.3.1 VPP – one-photon micro-stereolithography (OμSL)

Compared with conventional SLA additive manufacturing methods, OμSL offers significantly higher resolution, enabling the fabrication of products with micron or nanoscale features [97, 98]. As a novel 3D printing technique, the classification of OμSL remains unclear. As it utilises UV light penetration for the selective photopolymerization of monolayers (**Fig. 12(a)**), it is regarded as an area-by-area VPP method in this paper. Li et al. recently achieved a significant advancement in the additive manufacturing of fused silica glass, creating intricate sub-micron features using OμSL. The research team developed a transparent nanocomposite precursor composed of polyethylene glycol-functionalised silica colloidal nanoparticles. This approach facilitated the production of a transparent fused silica glass lattice with hierarchical structures ranging from millimetric to sub-micron scale details (**Fig. 12(b)**) [97], which could inspire the development of similar ceramic printing techniques.

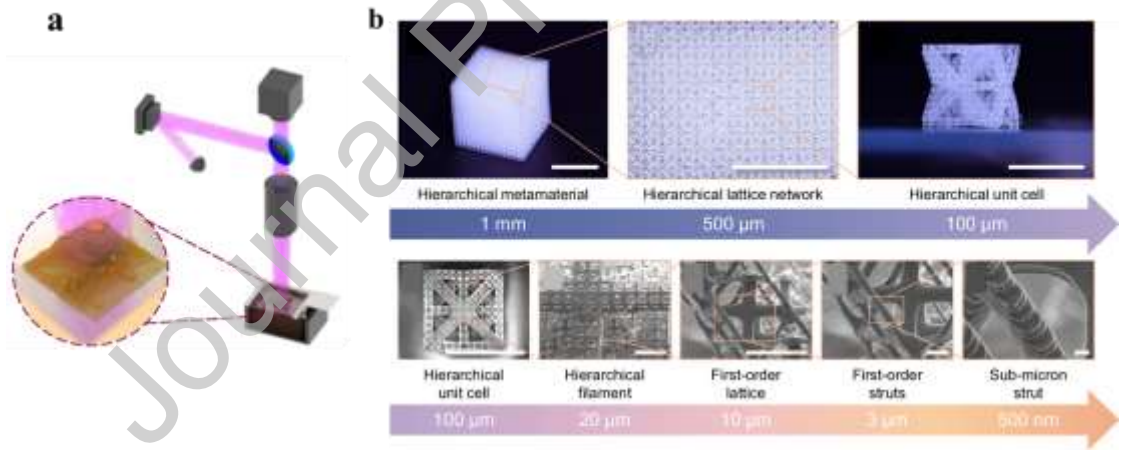

Fig. 12. OμSL: (a) Schematic; (b) Fused-silica glass hierarchical lattice structure printed via OμSL. [97]

2.3.2 VPP – digital light processing (DLP)

Although SLA and DLP are both most widely applied VPP techniques, compared with SLA, DLP cures an entire layer simultaneously using a digital light source instead of a laser while maintaining the high accuracy and surface quality characteristic of SLA [2]. This technology has

attracted significant attention from Chinese research groups. For example, Li et al. utilised DLP to manufacture intricate lattice structures from SiOC ceramics. They developed a precursor by blending polysiloxanes with photosensitive acrylate monomers, resulting in SiOC ceramics with both high strength and lightweight properties [99]. Furthermore, the research team improved the mechanical properties of octet-truss structure SiOC ceramics through metal doping, enhancing the pinning effect [100]. Elsewhere, Zhang et al. comprehensively investigated the mapping relationship between the content of zirconia slurries and their rheological properties and stability. It was discovered that ink printability was optimised with a dispersant content of 3.5 wt%. Based on a careful analysis of the microstructure, surface and topological properties of zirconia ceramic slurries and their relationships with mechanical properties, micro-ceramic gears with exceptional performance were fabricated by controlling the shrinkage rate of the solid load of $ZrO_2(3Y)/Al_2O_3$ ceramics [101]. Inspired by biological core–shell structures, a cellular ceramic structure/polyurea dual-phase architecture was proposed by Zhang et al. and fabricated via DLP and infiltration technologies. The architecture was proven to have exceptional endurance for cyclic loading [102]. The versatility of DLP has been demonstrated in its compatibility with various types of ceramic materials, including alumina [103], aluminium nitride [104], cordierite slurries [105], titanium dioxide [106], zirconia ceramics [107], and others.

DLP has also demonstrated its compatibility with bioceramics, with numerous studies focusing on fabricating porous bioceramic scaffolds [108-111]. In 2021, Liu et al. utilised the Voronoi tessellation method to design novel biomimetic porous scaffolds with trabecular-like morphology, employing beta-tricalcium phosphate (β-TCP) as the material. DLP technology enabled the programmable adjustment of porosity and pore size in these scaffolds, with porosities ranging from 45% to 75% (**Fig. 13(f)**). Pore sizes could also be tailored from 360 μm to 1200 μm [112]. Elsewhere, Liu et al. mixed β-TCP with photosensitive acrylate resin, resulting in a ceramic slurry system with a low viscosity and high solid content [113]. More recently, Guo et al. employed a Pickering emulsion feedstock to produce hierarchical porous hydroxyapatite scaffolds with complex geometries and pore sizes ranging from millimetres to <10 μm. Characterisation of these scaffolds revealed a remarkable compressive strength of up to 8.03 MPa at 72.96% porosity [114]. Additionally, Wang et al. introduced 5.5% mono-alcohol ethoxylate phosphate to the calcium phosphate (CaP) powders for DLP printing, resulting in a slurry with high solid loading and low viscosity. This modification enabled the successful preparation of scaffolds with various lattice structures, including cube, octet-truss, and inverse face-centred cubic (fcc) [115].

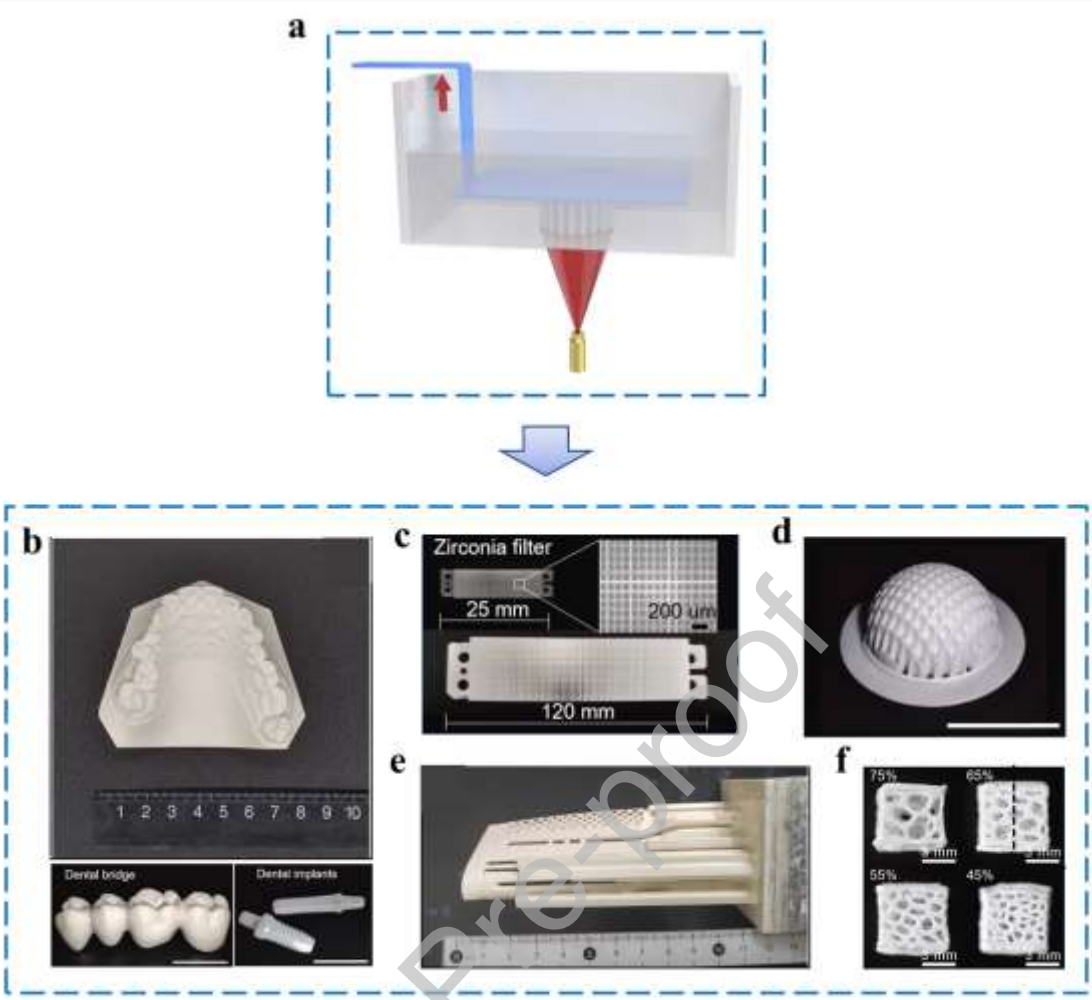

Fig. 13. Wide-ranging applications of ceramic structures printed by DLP: (a) Schematic of DLP [2]; (b) Dental structures and implants, scale bars: 10 mm [107, 116]; (c) Zirconia filter [107]; (d) Dome structure, scale bar: 10 mm [107]; (e) Aero-engine blade core [116]; (f) 3D Voronoi-based scaffolds with tailored porosity in bone tissue engineering [112].

Efforts to address the inherent shortcomings of the DLP technique have been vigorous. Hu et al. noted that excess cured areas resulting from light scattering compromised the accuracy of DLP-printed ceramic components. To tackle this issue, the team investigated various printing parameters, such as the feed rate and feed height. They discovered that manipulating the shear stress strategically could eliminate these excess cured areas. Moreover, their experiments showed that by controlling shear stress, the relative forming error for small features could be dramatically reduced by 51.66% [117]. Hu et al. devised a cyclic process of DLP manufacturing involving coating, exposure, cleaning, and drying stages. This process effectively addressed the challenges associated with the integration of multiple ceramics in DLP printing. **Fig. 14(a)** depicts three components with multi-

ceramic distribution within and between layers. The layers were devoid of defects and exhibited high precision [118]. Furthermore, Cheng et al. developed a novel method for large-volume multi-material printing, utilising centrifugal force to enable non-contact, high-efficiency material switching. Based on the centrifugal multi-material 3D printing method, the team successfully fabricated a ceramic spider and a ceramic bearing with elastomer supports. The ceramic bearing was then employed in a turbine, and a flame impact test revealed that it could withstand working temperatures as high as 650 ℃. This technique has also proven feasible for other materials, including hydrogels and polymers [119].

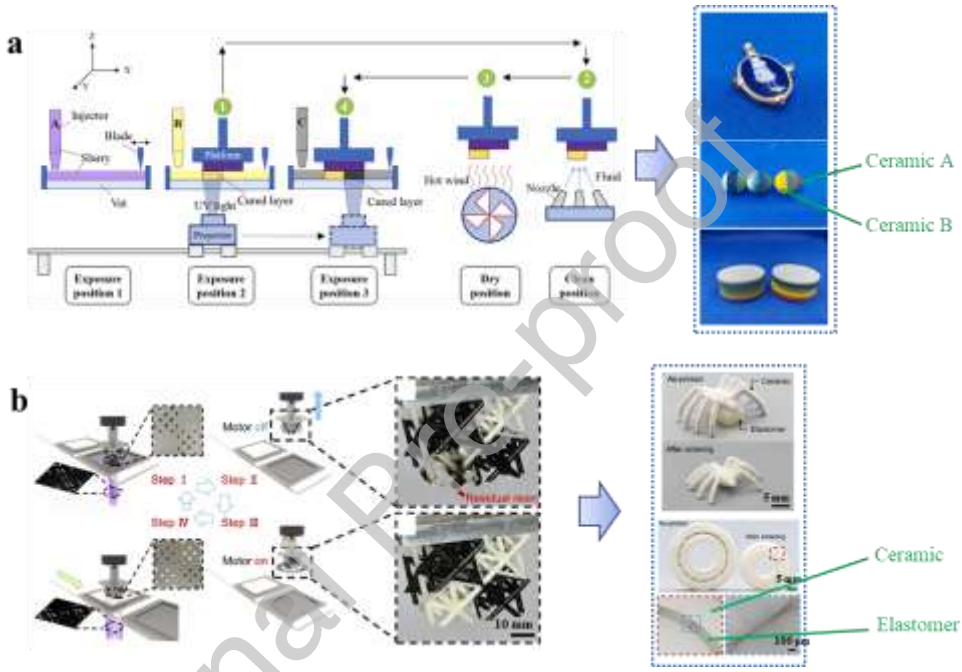

Fig. 14. Methods for DLP printing multi-material ceramic parts: (a) Schematic of coating, exposure, cleaning, and drying stages for a multi-material DLP process, as well as a cartoon 3D structure, hollow multi-ceramic balls, and multi-ceramic porous structures fabricated via such a cyclic process [118]; (b) Schematic of the centrifugal multi-material DLP method and ceramic-elastomer products, including a spider and a bearing [119].

The mechanical and thermal properties of ceramics produced via DLP can be enhanced through various means. In situ mullite has shown effective reinforcement of alumina-based ceramic cores. Reducing the doping level of fused silica and adjusting the sintering temperature can increase the porosity of reinforced cores. Optimal properties were achieved with a 20 wt.% fused silica doping and a sintering temperature of 1673.15 K, resulting in ceramic cores with 40% porosity and a bending strength of 25 MPa at 1773.15 K [120, 121]. Wu and colleagues concentrated on enhancing

the mechanical and thermal properties of aluminium nitride (AlN) ceramics. The addition of KH570 surfactants to the AlN suspension led to reduced viscosity and improved stability. With a solid loading of 50%, the ceramics reached a peak thermal conductivity of 150 W/mK and a flexural strength of 401 MPa [122]. The researchers also explored another strategy that involved the powder coating of an yttrium aluminate layer. This method yielded a thermal conductivity and bending strength of 144.11 W/mK and 400.07 MPa, respectively, surpassing those obtained through conventional preparation methods [123]. Elsewhere, Hu et al. introduced 5 wt% MgO into titania ceramic slurry, which generated a $MgTi_2O_5$ material that filled the voids in titania grains, resulting in an optimised bending strength of 71.9 MPa [124].

The light transmittance of LuAG: Ce can reach ~40%. **Fig. 15(b)** illustrates a superhemispherical ceramic device crafted from LuAG: Ce. The device exhibited exceptional laser-driven lighting properties. The printing resolution of this process reached 50 μm [125]. Chen et al. achieved the successful fabrication of complex structures of $Si_3N_4 - SiO_2$composite ceramics with excellent wave-transparent performance [126]. In addition to transparent ceramics, piezoelectric ceramic scaffolds made from barium titanate ($BaTiO_3$) can also be fabricated via DLP with controllable porosity [127]. Moreover, Zhou et al. developed a novel UV-curable polysiloxane precursor with good printability, which could be used to print cross-helix array ceramic metamaterials with exceptional electromagnetic wave (EM) absorption performance [128]. Similarly, significant achievements have been made in the DLP fabrication of a wide range of ceramic metamaterials with exceptional and tuneable electromagnetic absorption features [129-134].

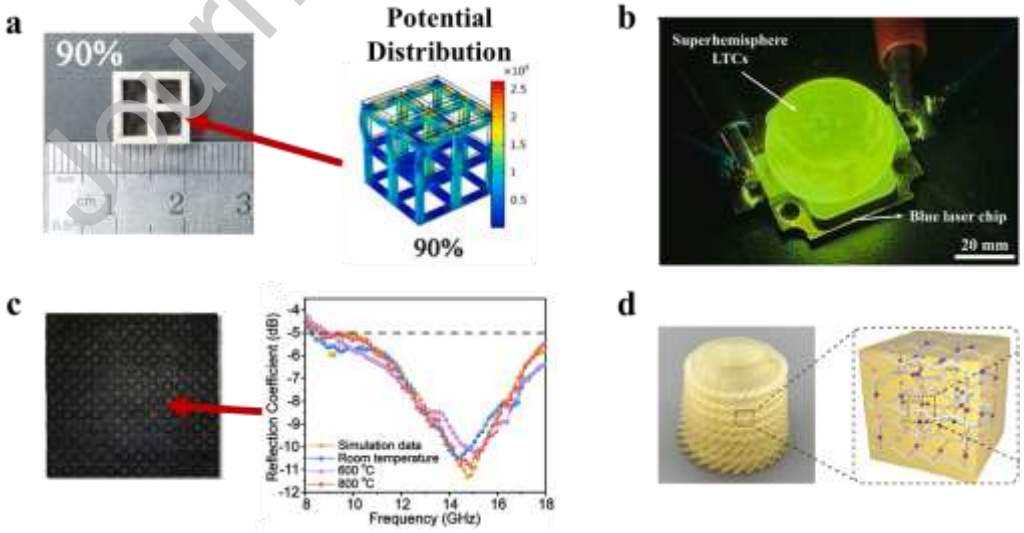

Fig. 15. DLP-manufactured ceramics with unique features: (a) Piezoelectric $BaTiO_3$ scaffold with 90% porosity and its potential distribution under 100 MPa pressure [127]; (b) Superhemisphere made from luminescent transparent ceramics (LTCs) [125]; (c) and (d) SiOC ceramic metastructure

with extraordinary EM absorption ability and a booster blade made from it [128].

2.3.3 Sheet lamination (SHL)

LOM is a subdivision of SHL additive manufacturing technique that employs layer-by-layer construction of objects using sheet materials, involving the bonding and adhesion of laser-cut thin sheets. LOM minimises the deformation and distortion of products owing to low thermal stress, although the strength between layers may be noticeably compromised. Zhang et al. prepared porous alumina structures using a novel frozen-slurry-based LOM technique (**Fig. 16(b)**). In their study, water, alumina powder, and organic binder were mixed to form a slurry. The frozen slurry facilitated pore formation with improved uniformity and orientation arising from the ice crystals. Nevertheless, reducing the layer thickness of the manufactured porous structures remains a challenge [135]. Another viable approach proposed by the researchers involves the use of an organic mesh sheet as a sacrificial material. As illustrated in **Fig. 16(c)**, a nylon mesh was laid prior to the application of the alumina slurry. Each layer was subjected to a drying process to enhance paving density and prevent delamination. Subsequently, the nylon mesh embedded within the green body was removed during degreasing and sintering, allowing pores to form within the alumina structure [136].

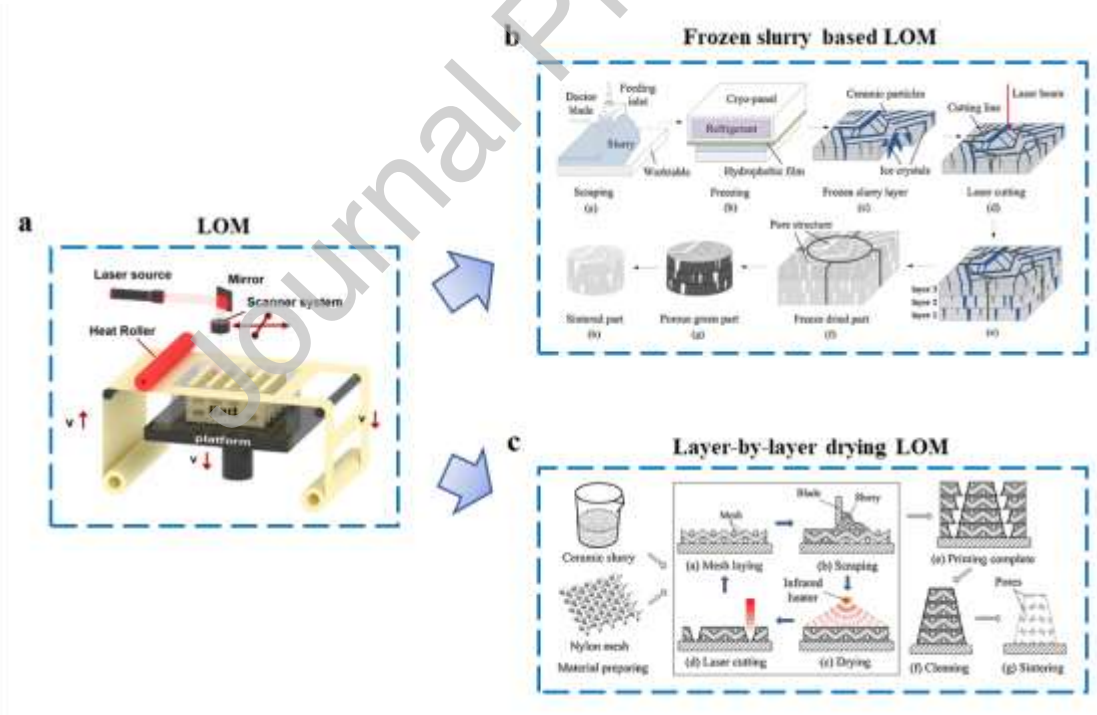

Fig. 16. Diagram of different LOM manufacturing processes: (a) Schematic of conventional LOM [1]; (b) Frozen slurry-based LOM [135]; (c) Layer-by-layer drying LOM [136].

2.4 Summary

Table 2 summarises and compares the materials, printing parameters, properties, and applications of different additive manufacturing methods. It can be observed that the printing speed of dot-by-dot methods commonly ranges within 4–10 mm/s, while those of line-by-line methods, such as DIW and FDM, generally range within 8–60 mm/s. SLA and PBF, which utilise light or laser scanning, can achieve even higher printing speeds exceeding 2000 mm/s. It is evident that line-by-line methods exhibit faster printing speeds than dot-by-dot methods.

For area-by-area methods such as DLP, an entire layer is printed simultaneously, and the layer exposure time is commonly within 1–30 s. Considering that the printing time for a single layer can be significantly affected by factors such as surface geometry, printing paths, speed changes, and nozzle movements in line-by-line methods, it is challenging to compare the speeds of area-by-area methods directly with those of line-by-line methods. However, it is reasonable to assume that area-by-area methods have a much higher printing speed, as they typically print a layer within seconds.

Table 2. Comparison of different additive manufacturing methods for ceramics. For studies in which resolution is not specified, nozzle diameter (for methods such as DIW and FDM) and layer thickness (for methods such as SLA and DLP) are assumed as the resolution. Printing speeds: printhead moving speed (MJT, BJT, DIW and FDM); scanning speed (SLA, PBF and DED); single layer exposure time (OμSL and DLP).

Additive manufacturing techniques		Base materials	Printing speed	Resolution (μm)	Scalability (cm)	Configuration	Mechanical properties	Other properties	Applications	Ref. No.
Dot by Dot	MJT	HA	4-10 mm/s	110-800	1.5	Scaffold; Mandible sample	Compressive strength – 5.5 MPa (60% porosity)	/	Bone tissue regeneration	[13]
		CaP	4-10 mm/s	110-800	1	Implanted scaffold	/	/	Skull bone tissue reconstruction	[14]
		LSCF and GDC	/	35	/	/	Elastic modulus – 93.56 GPa; Hardness – 2.14 GPa	/	SOFCs	[9-11]
		α-Al_2O_3	/	40	1	/	Compression strength – 89 MPa; Flexural strength –	Relative density – 95.2%; Surface roughness – 3.7 μm;	Circuits-on-ceramics	[12]

						49.4 MPa; Vickers hardness – 291.6 Hv	Volume shrinkage rate – 32%		
		SiO_2-H_3BO_3	/	150 dpi	2.5	University badge; Shaped part	/	Dielectric constant – 2.485; Dielectric loss – 0.0038 (1 MHz)	Ceramic electronics on curved substrates	[15, 16]
		ZrO_2	/	20	2.5	Final parts; model, support and envelope structures	Flexural strength – 699 ± 104 MPa; Fracture toughness – 7.52 MPa $m^{1/2}$; Hardness – 12.43 GPa	Linear shrinkage – 17.47%; Relative density – 99.5%; Surface roughness – 0.33 μm	/	[17]
	BJT	ZrO_2	6000 mm^2/s	5760 × 1440 dpi	/	/	Flexural strength – 307 MPa	Linear shrinkage – 23.93%; Relative density – 75.01%; Surface roughness – 7.69 μm;	/	[24]
		Si-SiC	/	100, 150, 200, 250	10	Optical mirror, turbine disc, and topology.	Compressive strength – 7.7 MPa; Flexural strength – 257 MPa	Porosity – 31.0-43.4%	/	[19]
		Al_2O_3	/	80	/	/	Flexural strength – 26.9 MPa	Linear shrinkage – 4.89-17.53%; Relative density – 70.05%	/	[20]
		Al_2O_3	/	50	8	Ceramic cores	Flexural strength – 79 MPa	Linear shrinkage – 13%; Relative density – 51%	Ceramic cores	[21]
		Al_2O_3	/	100	2.5	Rectangular block	Compressive strength – 58.7 MPa	Linear shrinkage – 37%; Relative density – 83.3%	/	[22]
		Al_2O_3	/	1080 × 1200 dpi	16	Gears and turbine blades	Flexural strength – 1.87 MPa	Density – 2.377 g/cm^3; Porosity – 39.34%	/	[25]
		CaO/ $CaZrO_3$	/	5760 × 1440 dpi	8	Rectangular block	/	Relative density – 41.7%	/	[23]
Line by Line	DIW (MEX)	TZP	8 mm/s	510	2	Dome structure	Vickers hardness – 14.583 GPa	Mid-infrared transmittance – over 70%; Relative density – 99.85%;	New laser materials and hierarchical optical windows	[47]
		$Al_{18}B_4O_{33}$	10 mm/s	10^3	5	Hierarchical pore structures	/	/	Catalyst support	[38]
		CaP	10 mm/s	400	0.6	Biomimetic wood porous scaffold	/	/	Modulate cellular behavior and osteoinductive activity	[41]
		Cordierite	10-15 mm/s	210	2.5	Honeycomb structures	/	/	Volatile organic pollutants removal technology	[37]

Al_2O_3	1 mm/s	100	0.9	Periodic lattice	/	/	/	[34]
Al_2O_3	3 mm/s	400	8	Bowl and impeller	/	/	/	[35]
Al_2O_3	15 mm/s	600	5.5	Lattice structures and porous catalyst carriers with biomimetic vein structure	Crush strength – 54.453±7.359 N/cm;	Methane conversion – 41.27%; Porosity – 60.03%; Specific surface area – 109.870 m^2/g	Catalyst carriers	[39]
Si_3N_4	10 mm/s	1.2×10^3	18	Single-wall cone	/	Linear shrinkage – 4.9-7.4%; Relative density – 54.3%	/	[30]
Si_3N_4	5-20 mm/s	90	/	Microchannel structures	/	/	/	[29]
Si_3N_4	/	10^3	/	/	Flexural strength – 348 MPa	/	/	[28]
Boehmite	20 mm/s	1.29×10^3-1.98×10^3	4	Lattice with hierarchical pore structure	/	Specific surface area – 400 m^2/g	Biomedical field, construction, industries, aerospace and environment treatment	[31]
CeO_2	20 mm/s	1.98×10^3	4	Hierarchically porous scaffolds	Compressive strength – 20 MPa (81% porosity)	/	Filtration, lightweight structural components, oxidative catalysis and oxide fuel cells, etc.	[32]
SiC	10 mm/s	210	3.2	Scaffold samples	Tensile strength – 21.3 MPa	/	/	[44]
SiC	15 mm/s	340	/	/	Compressive strength – 390 MPa (41.3% porosity)	/	/	[43]
SiC	1-20 mm/s	100, 150, 200, 400	2	Carious 3D structured lattice	/	/	/	[36]
SiOC-ZrO_2	10-50 mm/s	200	10	Origami (butterfly, Sydney opera house, rose, and dress); Miura-ori design; bending, helical ribbon, and saddle surfaces; cellphone back plate; curved honeycomb	Compressive strength – 547 MPa	4D printing elastomer-derived ceramics	Autonomous morphing structures, aerospace propulsion components, space exploration, electronic devices, and high-temperature microelectromechanical systems.	[50]
SiOC-ZrO_2, SiOC-AlON	/	6 (DIW + laser engraving)	16	Turbine blisk, Kirigami (flower, stars), calligraphy characters, Flying Apsaras, MEMS, and bending structure	/	4D printing elastomer-derived ceramics; 4D additive–subtractive manufacturing of ceramics; 4D printing shape memory ceramics	High-temperature structural materials in the aerospace, electronics, biomedical, and art fields	[51]

	SiOC-ZrO_2, SiOC-AlON	/	< 28 (DIW + laser engraving)	> 8	Butterfly-shaped jewelry; cross, Tachi and panda patterns; calligraphy characters; MEMS; bending and saddle surface	/	4D printing elastomer-derived ceramics; 4D additive–subtractive manufacturing of ceramics	High temperature MEMS, jewelry and art decorations	[52]
	SiOC	/	200	1.4	Grid structure with tailored porosity	Yield strain – 70%	Linear shrinkage – 25%	/	[33]
	AlON	/	/	1	Ceramic tiles	Fracture toughness – 1.74 MPa $m^{1/2}$; Vickers hardness – 18.56 GPa	Transmittance – 81.90% (780 nm wavelength)	/	[45]
	$BaTiO_3$	/	0.46	/	Scaffold of the woodpile structure	/	/	Piezo-photoelectric catalytic	[48]
	PZT	/	210, 260	1.8	Annulus and ribbon spiral structures	/	Relative density – 98%; Piezoelectric constant – 265 pC/N	/	[49]
FDM (MEX)	Whitlockite	8 mm/s	/	1.5	Scaffolds	/	/	Regeneration of neuro-vascularized bone tissue	[60]
	Si_3N_4	25 mm/s	600	6	Turbine rotor, gear and swirl fan	Flexural strength – 824.74 MPa	/	/	[54]
	ZrO_2	40 mm/s	600	10	Curved surface structures (fish, honeycomb, parts, topology)	/	/	/	[56]
	PLA	< 50 mm/s	1.75×10^3	0.63	Scaffolds	Elastic modulus – 47 MPa	/	Regeneration of hard tissues	[53]
	PLA/HA	60 mm/s	1.75×10^3	1	Scaffolds	/	/	Bone repair scaffolds	[59]
	TZP	/	200, 400, 600, 800, 10^3	6	Gear body, turbine rotor, dental crowns, screws and nuts	Flexural strength – 890 MPa	/	/	[55]
	SiC	/	200, 400	1.9	Honeycomb structure	Tensile strength – 471 ± 54 MPa	/	/	[57]
PBF	Al_2O_3/ZrO_2	0.05-0.3 mm/s	300	7	Bar samples	Fracture toughness – 4.5 MPa $m^{1/2}$; Hardness – 16.7 GPa	/	/	[66]
	Al_2O_3/$GdAlO_3$/ZrO_2	100-450 mm/s	100	3	Different shapes such hexagonal prisms	/	/	Industrial and manufacturing engineering.	[67]
	Mullite	1600 mm/s	130	3	Different gear structures	Compressive strength – 6.7 MPa;	Linear shrinkage – 14.4%; Porosity – 79.9-88.7%	/	[72]

	SiO_2	1800 mm/s	100	50	Ceramic core	Flexural strength – 17.21 MPa; Flexural strength at 1550 ºC – 13.90 MPa; Creep deformation – 0.32 mm	Linear shrinkage – 2.37%; Porosity – 28.39%	Ceramic core for hollow turbine blades.	[63]
	Si/SiC	2000 mm/s	100	2	SiC-based TPMS structures	Compressive strength – 16.3 MPa; Elastic modulus – 932.0 MPa	Linear shrinkage – 6%;	/	[68]
	C_f/SiC	2000 mm/s	100	/	/	Flexural strength – 249 MPa; Fracture toughness – 3.48 MPa $m^{1/2}$	Density – 2.83 g/cm^3; Linear shrinkage – 3%	/	[69]
	SiC	1700-2300 mm/s	100, 200, 250	4.5	Twisted loop and impeller structure	Bending strength – 348 MPa	Density – 2.94-2.98 g/cm^3	/	[70]
	Al_2O_3	1800 mm/s	130	/	/	Compressive strength – 0.72 MPa;	Linear shrinkage – 13.10-14.03%; Porosity – 72.41%	Ceramic foams with complex structure and high porosity	[73]
	Al_2O_3	4000 mm/s	100	28	Integral ceramic mould	Flexural strength – 13.03 MPa	Linear shrinkage – 1.5-2.03%; Porosity – 30.82%;	Integral core and shell for hollow turbine blades	[62]
	Al_2O_3	2000-4000 mm/s	150	6	catalyst carriers with porous structures	Crush strength – 45.88 N/cm	Porosity – 72.88%; Specific surface area – 56.324 m^2/g;	Catalyst carriers	[65]
	Al_2O_3	/	150	12	Leaf vein structure catalyst carriers	Crush strength – 86.03 ± 18.10 N/cm	Porosity – 64.85%; Specific surface area – 1.958 cm^2/g	Petrochemical industry	[64]
DED	Al_2O_3/ $GdAlO_3$/ ZrO_2	1.6 mm/s	80	12.5	Rod sample	Hardness – 15.84 GPa	/	/	[79]
	Al_2O_3/ $GdAlO_3$/ ZrO_2	1.6 mm/s	80	25	Rod sample	/	/	/	[78]
	Al_2O_3/ $GdAlO_3$/ ZrO_2	0.8-3.2 mm/s	100	9	Rod sample	/	/	/	[74]
	Al_2O_3/ ZrO_2	5.8 mm/s	400	4	Cylindrical samples	Flexural strength – 160.19 MPa	/	/	[77]
	Al_2O_3/ ZrO_2	6.7 mm/s	400	4.5	Cylindrical samples	Compressive strength – 480.76 MPa; Flexural strength – 226 MPa	Porosity – 0.29%	/	[76]
	Al_2O_3/	5-7.5	/	7	Arc-shaped and	/	Porosity –	/	[75]

	ZrO_2	mm/s			cylindrical structures		0.1±0.05%; Relative density – 99.9%		
	LRS	1200 mm/s	100	2.5	Gear, turbine blade, and coupling structures	Compressive strength – 444.23 MPa; Flexural strength – 132.21 MPa	Density – 2.73 g/cm^3; Porosity – 3.12%	Lunar regolith printing	[86]
	Al_2O_3	2500 mm/s	50	9	Ceramic cores	Flexural strength – 50.1 MPa; High temperature deflection – 2.27 mm	Porosity – 36.4%	Hollow turbine blades ceramic cores	[80]
	Al_2O_3	/	40	1.6	TPMS structures	Compressive strain – 50%	Relative density – 14-37%	/	[90]
	Diatomite	2500 mm/s	50	4.5	Different macropore structures	/	Porosity – 50.29-56%	/	[89]
	SiO_{2f} /SiO_2	2500 mm/s	/	15	Cambered structure	Compressive strength – 51.2 MPa; Flexural strength – 24.3 MPa;	/	/	[93]
SLA (VPP)	Biphasic calcium phosphate	/	/	4	Scaffolds	Compressive strength – 370.03 MPa; Flexural strength – 133.19 MPa; Vickers hardness – 3.83 GPa	Density – 3.01 g/cm^3; Porosity – 51.49%	Bone tissue engineering	[81]
	SiC	/	50	4	Pyramid and hollowed basket	/	/	/	[84]
	SiC	/	/	1.3	Screws and nuts	Flexural strength – 462 MPa	/	/	[85]
	SiC	/	/	4	Lattice	Elastic modulus – 18.7 GPa; Flexural strength – 229 MPa; Hardness – 1.66 GPa	Density – 2.13 g/cm^3; Porosity – 10.2%	/	[88]
	ZTA	/	100	2	Dentoid parts	Flexural strength – 530.25 MPa; Fracture toughness – 5.72 MPa $m^{1/2}$; Vickers hardness – 17.76 GPa	Density – 4.26 g/cm^3;	/	[91]
	$MgAl_2O_4$	/	100-200	1.25	Lens	Vickers hardness – 13.5 GPa	Transmittance – 97%	Optical lenses/windows and photocatalyst supports	[94]

		PZT	/	/	/	Ultrasound 2D array	/	Dielectric constant – 760-1390 Piezoelectric constant – 212-345 pC/N	Piezoelectric ceramics	[95]
		ZrO_2 and Al_2O_3	/	50	4.4	Multi-ceramic QP-3 structures	/	Thermal expansion coefficient – -10^{-5}-10^{-5}/ºC	/	[96]
	OμSL (VPP)	SiO_2	2 s	0.5	0.15	Hierarchical metamaterial lattice	/	/	Micro-optics, microfluidics, mechanical metamaterials, and engineered surfaces	[97]
		MgO-TiO_2	20-30 s	1920 × 1080 dpi	4.5	Characters and scaffolds	Compressive strength – 18.2 MPa; Flexural strength – 71.9 MPa	/	Monolithic catalysts and tissue engineering scaffold	[124]
		TiO_2	12-75 s	200	0.5	Porous scaffold	Compressive strength – 1.50 MPa	Porosity – 50-80%	Bone tissue engineering, filters, radiators, etc.	[106]
		SiOC	6 s	25-100	18	Metastructure	/	/	Electromagnetic wave absorbing metamaterial	[128]
		SiOC	/	50	1	Designed lattice structures	Specific strength - 5.74×10^4 Nm/kg	Density – 0.33 g/cm^3;	/	[99]
		SiOC	/	50	1.5	Designed lattice structures	/	Density – 2.1 g/cm^3; Linear shrinkage – 35.4%; Relative density – 98.5%	Lattice-structured ceramics	[100]
Area by Area	DLP (VPP)	SiOC	/	30	/	/	Specific strength – 6.520×10^4 Nm/kg	Density – 0.550 g/cm^3; Effective absorption bandwidth – 6.11 GHz	Microwave-absorbing metamaterial	[129]
		ZrO_2	6 s	25	12	Logo, dome structure, dental bridge, dental implants, filter, and porous structure	Flexural strength – 1042 MPa; Fracture toughness – 6.68 MPa $m^{1/2}$; Hardness – 12.59 GPa	Linear shrinkage – 23%; Relative density – 99.71% Surface roughness – 1.62-2.86 μm;	Industry fabrication	[107]
		LuAG:Ce	6 s	50	1.1	Superhemispherical ceramic device	/	Transmittance – 40%	High-power laser-driven solid-state lighting devices	[125]
		SiBOC	6 s	100	2	Metastructure	Yield strain – 64.07%	Effective absorption bandwidth – 11.36 GHz	Microwave-absorbing metamaterial	[130]
		ZrO_2(3Y) /Al_2O_3	5 s	45	0.4	Gears	Compressive strength – 1900 MPa; Flexural strength – 648 MPa;	Relative density – 98.53%	Micro-ceramic gears	[101]

					Fracture toughness – 6.4 MPa $m^{1/2}$; Hardness – 13.40 GPa			
	Al_2O_3/polyurea	5 s	100	1.5	Dual-phase architecture	Cyclic life under 40.28 MPa – 120 cycles	/	/	[102]
	Al_2O_3	10 s	100	/	/	Flexural strength – 26.4 MPa	Density – 2.4 g/cm^3; Porosity – 42%	Ceramic cores	[121]
	Al_2O_3	5 s	100	/	/	Flexural strength – 25 MPa (1773.15 K)	Porosity – 40%	Ceramic cores	[120]
	SiBCN(O)	4-8 s	100	4	Metastructure	/	Electromagnetic wave absorption – 94.6% (Ku band), 100% (X band)	Electromagnetic wave absorbing metamaterial	[131]
	$BaTiO_3$	2.8 s	35	1	Porous structure	Flexural strength – 57.9 MPa	Piezoelectric constant – 241 pC/N; Porosity – 10-90%	Bionic bone scaffolds	[127]
	CaP	2 s	50	0.9	Octet-truss and inverse fcc lattice	/	/	Clinical regeneration and repair	[115]
	β-TCP	12 s	50	0.6	Trabecular-like scaffold	Compressive strength – 0.8-4.1 MPa	Porosity – 45-75%	Catalysis, heat insulation, fuel cell, etc.	[112]
	β-TCP	1-2 s	50	1	Scaffold	Compressive strength – 9.89 MPa	Porosity – 40%	Bone repair and regeneration	[113]
	AlN	/	/	1.3	Gear, lattice and porous structures	Flexural strength – 401 MPa	Thermal conductivity – 150 W/mK	/	[122]
	Si_3N_4-SiO_2	/	/	2.4	Lattice	Flexural strength – 77 MPa	Density – 1.60-1.76 g/cm^3; Relative permittivity < 4	/	[126]
	PyC/Al_2O_3	/	/	2.5	Micro-channel structure	/	Effective absorption bandwidth – 12 GHz	Microwave-absorbing metamaterial	[132]
LOM (SHL)	Al_2O_3	/	100	4	Inclined structures	Compressive strength – 42 MPa	/	/	[135]
	Al_2O_3	/	/	7	Gear	/	Porosity – 51.5%	SOFCs, biological scaffolds, and filter membranes	[136]

In addition to the aforementioned categories, volumetric additive manufacturing (VAM) has emerged as a novel 3D printing method. Whyte et al. construed VAM as a fabrication process whereby 3D objects could be constructed in a single step, instead of serial repetitions of lower-dimensional operations, by inducing changes in the in-situ material/medium without the need to add

new materials [137]. Compared with other additive manufacturing methods, VAM techniques allow for the simultaneous fabrication of 3D objects, effectively eliminating layer-induced defects. Furthermore, this manufacturing process requires no supporting structures, providing greater freedom in product design [138]. The printing speed of VAM commonly ranges from 2 mm^3/s to 110 mm^3/s, with the overall exposure time commonly within 10–400 s [137], indicating an even higher manufacturing speed than layer-by-layer methods. For instance, Toombs et al. proposed microscale computed axial lithography additive manufacturing, which utilises tomographic superposition for selective polymerisation. This method can fabricate fused silica with a high mechanical strength and resolution, achieving a minimum feature size of 50 μm. Complex structures with a scalability of approximately 0.8 mm were produced within 90 s, demonstrating a printing speed surpassing that of layer-by-layer methods [139]. It is anticipated that VAM could become the next research focus of ceramic 3D printing in China.

3. Ceramic 4D Printing

3.1 New material

4D printing involves 3D printing followed by a shape-morphing step under certain stimuli. The development of ceramic 4D printing has transitioned from the use of homogeneous precursors with elasticity to the use of heterogeneous precursors based on single- or multi-material printing (**Fig. 17**). In 2018, Liu et al. [50] developed a novel 3D printing 'ceramic ink' blending poly(dimethylsiloxane) (PDMS) and ceramic fillers. The resulting elastomer composites exhibited flexibility, stretchability, and the capacity for shape transformation, leading to the development of a new material class known as 4D printing elastomer-derived ceramics (4DP-EDCs). This shape transformation was achieved through prestrain-induced compressive buckling or self-shaping, during which the previously stored elastic energy in the precursor material was released to serve as the driving force. In 2019, this innovative work gained international recognition, as it was among the four 4D printing breakthroughs highlighted by the European Commission in its '100 Radical Innovation Breakthroughs for the Future' report and was hailed as 'the world's first-ever 4D printing for ceramics' [140]. The majority of innovations featured in the abovementioned document were from European and American countries, with only 3.7% originating from China. Furthermore, Chinese cases accounted for a mere 0.7% of the listed innovations granted US patents, underscoring the significance of this pioneering ceramic 4D printing achievement published in 2018 [50] (**Fig. 18**).

The 4D printing of EDCs has enabled breakthroughs in the geometric flexibility of ceramics, introducing novel possibilities for versatile ceramic 4D printing techniques. Liu et al. [51, 52] proposed a pioneering approach for fabricating 4D-printed EDCs using heterogeneous precursors derived from single- or multi-material printing and achieved a seamless shape and material transformation. The heterogeneous precursor was generated through UV/ozone treatment on the surface of the printed homogeneous precursor or via multi-material printing with different 'ceramic inks'. The heterogeneous precursor was then subjected to a heat treatment process. The mismatch in thermal expansion behaviours among the precursor materials induced a first-stage shape transformation, and the discrepancy in thermal shrinkage behaviours triggered a second-stage shape transformation (**Fig. 17**). The thermal expansion behaviour is characterised by distinct yet cohesive thermal expansion-dominated shape transformations from UV/ozone-treated precursors [51] and thermal shrinkage-dominated transformations from multi-material-printed precursors [52]. This reveals the potential of deriving multiple variants from the thermal expansion–shrinkage balance or other types of expansion–shrinkage balances, such as room-temperature expansion/shrinkage behaviours.

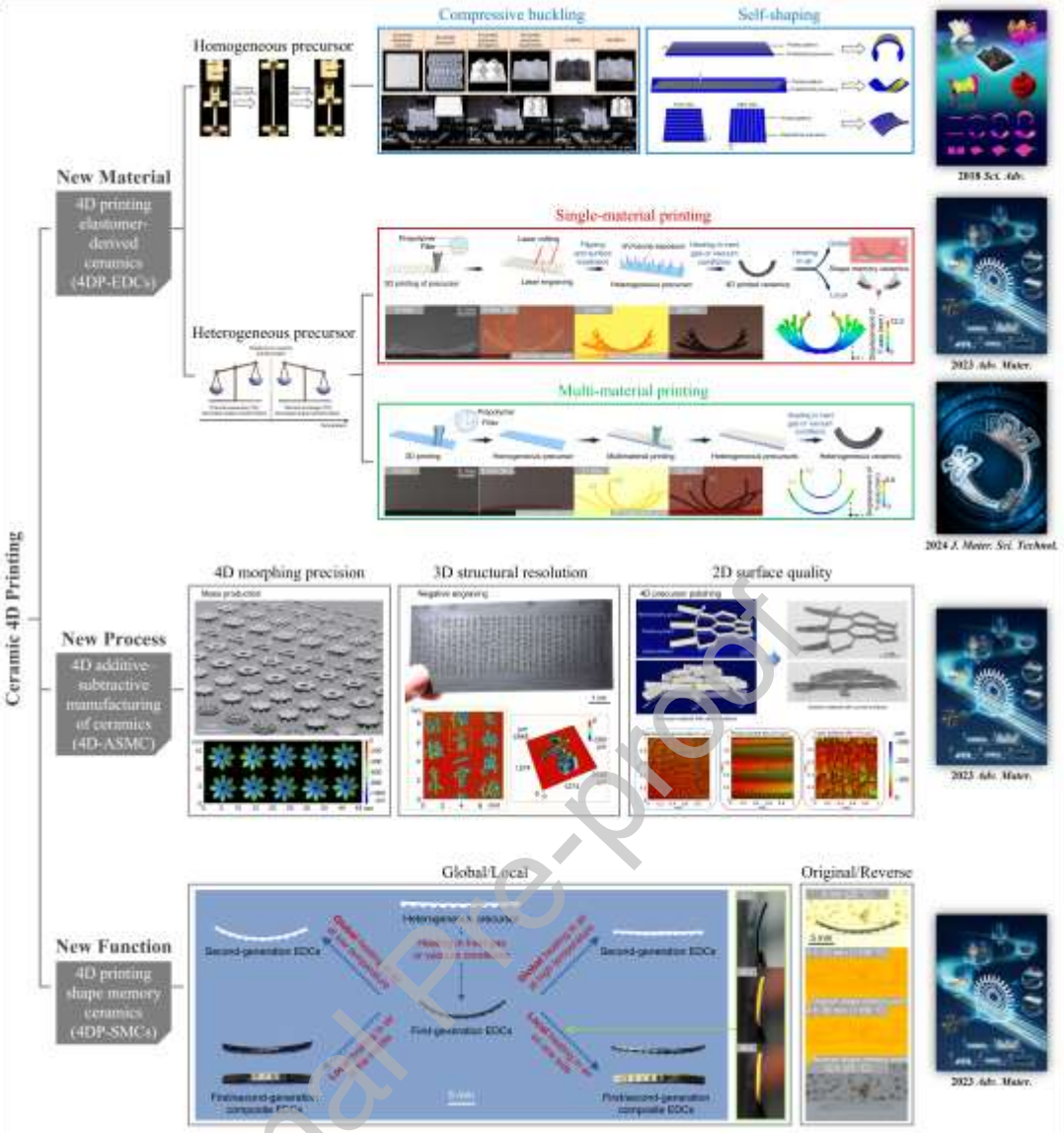

Fig. 17. Milestones in current ceramic 4D printing. [50-52]

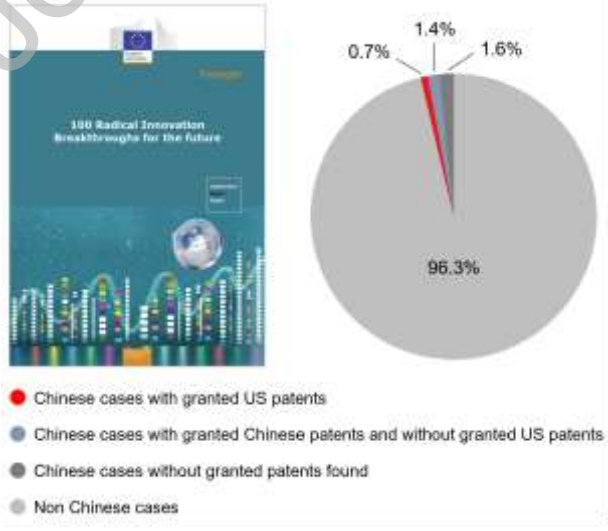

Fig. 18. Statistics on the '100 Radical Innovation Breakthroughs for the Future' by the European Commission [140].

Moreover, to reduce the limitations in the thermal stability for 4D printed SiOC-based crystalline-amorphous dual-phase (CADP) ceramic materials, Liu et al. explored the mechanism of atomic layer deposition (ALD)-ed Al_2O_3 on the flame ablation performance of the printed SiOC-based CADP ceramic lattice structure, and demonstrated the significant improving effect resulting from the Al_2O_3-rich layer in the high-temperature performance of 4D printed lightweight and complex structural ceramics [51]. Compared to the typical bulk IN718 alloy enhanced with physical vapor deposition (PVD)-ed thermal barrier coating (TBC) [141], ALD-ed 4D printed ceramic lattices exhibited a six times higher flame ablation performance [51] (**Fig. 19**).

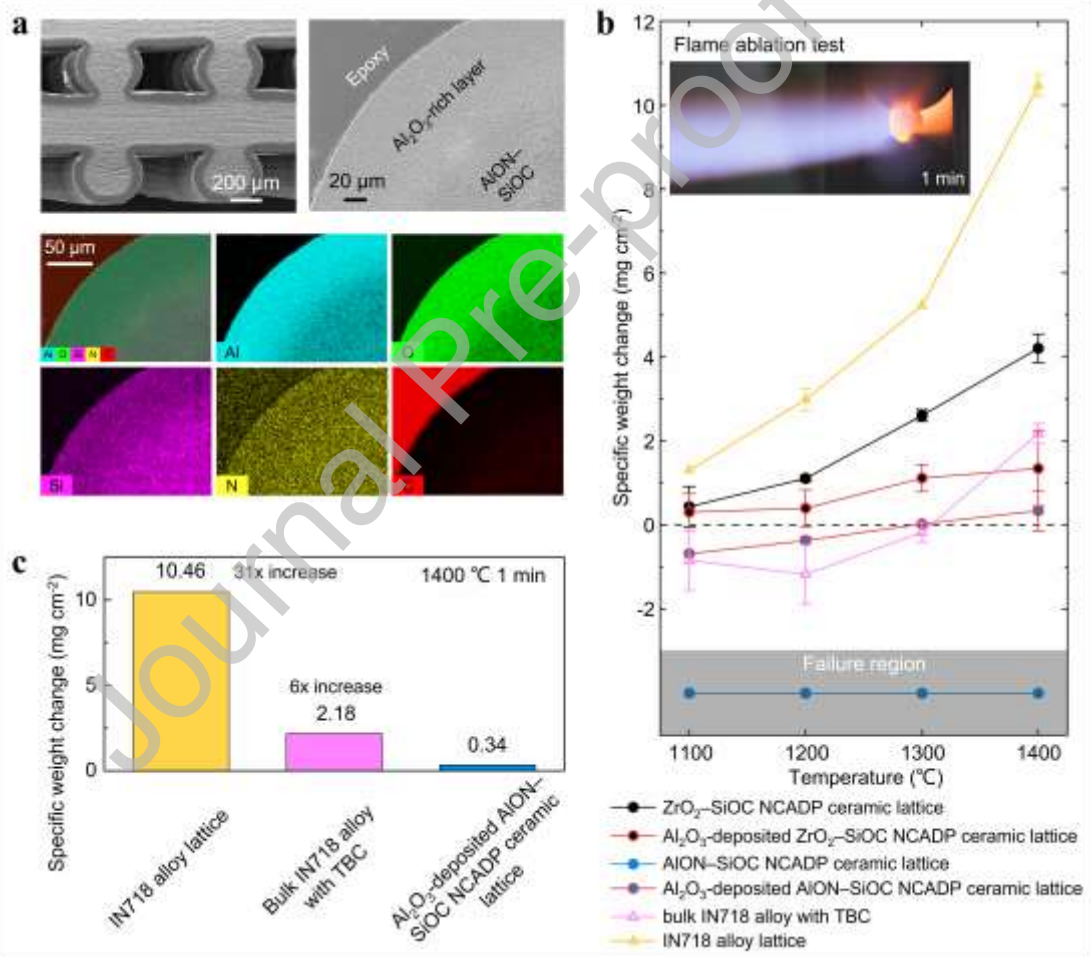

Fig. 19. Thermal performance of 4D printed SiOC-based CADP ceramic materials: (a) SEM images showing the uniformly Al_2O_3-rich layer generated on the surface of the printed ligaments in the interior of the ceramic lattices; (b) Flame ablation tests illustrating the improving effect resulting from the Al_2O_3-rich layer; (c) Comparison with IN718 alloy and bulk IN718 alloy with TBC [51].

3.2 New process

The origins of additive–subtractive manufacturing of ceramics can be traced back to ancient China (**Fig. 20(a)**). During the early period, various techniques such as 'Louhua' (manual cutting), 'Kehua' (manual engraving), 'Tihua' (manual negative/positive engraving), and 'Tiaodao' (semi-automatic engraving) were used to machine the green body of ceramics. Laser subtractive manufacturing of inelastic precursor materials, integrated with computer-aided manufacturing of laminated engineering materials (CAE-LEM) [142] and LTCC [143] to generate high-resolution ceramic structures emerged around the year 2000. Recently, Liu et al. utilised elastic precursors to introduce a new process called 4D additive–subtractive manufacturing of ceramics (4D-ASMC). Laser cutting/engraving/polishing of elastic precursors contributes to improved 2D/3D/4D manufacturing resolution in aspects such as 2D surface quality, 3D structural resolution, and 4D morphing precision (**Fig. 17**) [51]. Studies have demonstrated the potential of 4D-ASMC as a versatile process for ceramic 4D printing, accommodating precursors from single- [51] and multi- [52] material printing (**Fig. 20(b)**).

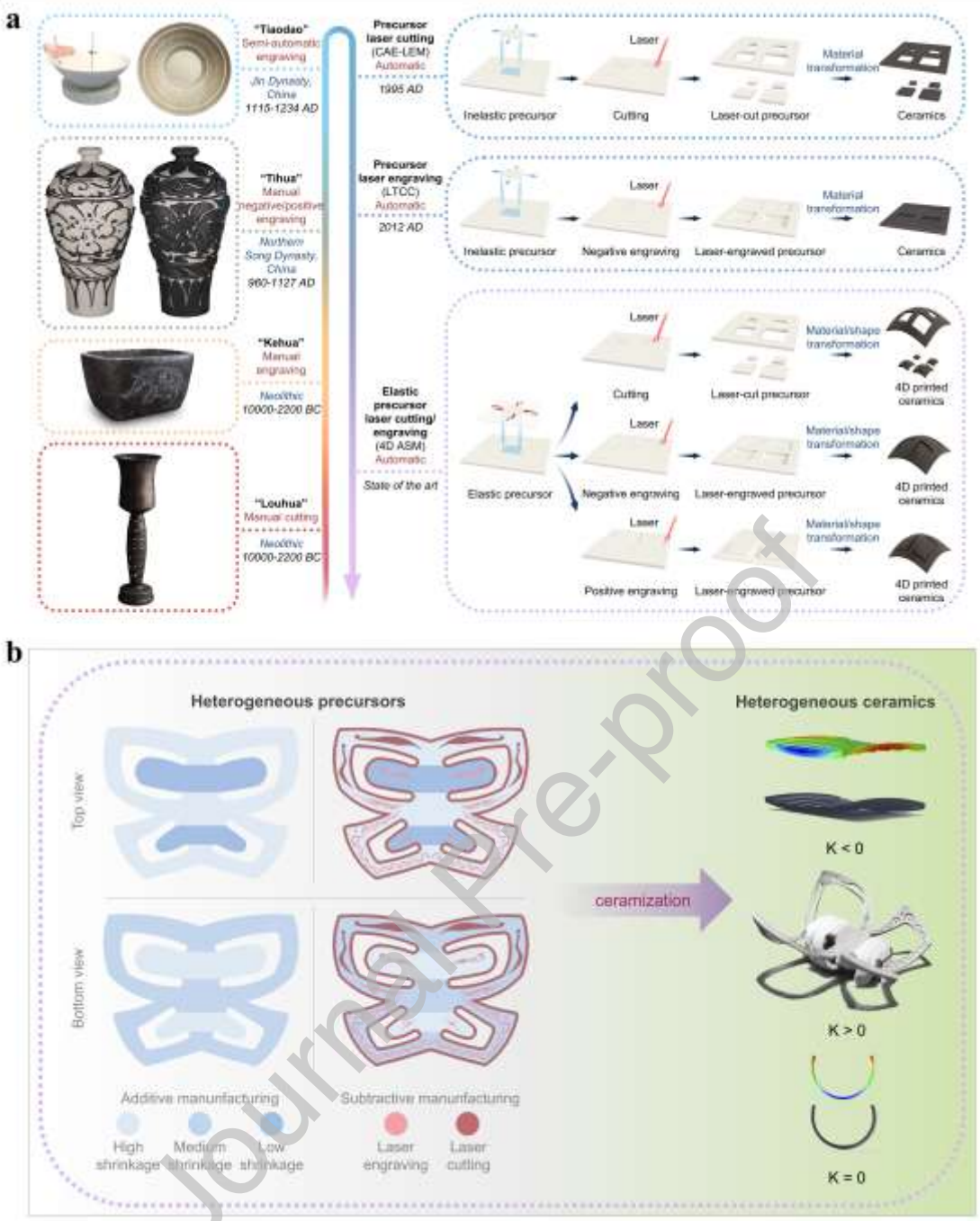

Fig. 20. 4D ASM of ceramics. (a) Inspiration from Chinese traditional ceramic arts [51]; (b) Demonstration with butterfly-shaped heterogeneous ceramics [52].

3.3 New function

4D-printed shape memory ceramics (4DP-SMCs) are among the successful variants derived from thermal expansion–shrinkage balance in ceramic 4D printing. Upon the heating of the first-generation EDCs, which originated from heterogeneous precursors exposed to UV/ozone treatment,

their thermal shrinkage behaviour diversity induced further shape transformation during re-ceramisation into second-generation EDCs (**Fig. 17**) [51]. The extent of this additional shape transformation could be adjusted through the variation of the heating temperatures: the application of higher heating temperatures to the first-generation EDCs resulted in a closer restoration to the original precursor shape, and in some cases, even a reversal to the shape of the first-generation EDCs in the resulting second-generation EDCs. Furthermore, localised heat treatment of the first-generation EDCs provided flexible and customisable local shape memory functions in the resultant first/second-generation composite EDCs. In summary, this new heterogeneous engineering strategy for preparing ceramic precursors by UV/ozone exposure has introduced a new function of 4DP-SMCs, offering original/reverse and global/local multi-mode shape memory capabilities in macroscale ceramics. This achievement stands apart from previous notable works focused on martensitic phase transformation-induced SMCs (**Table 3**).

Table 3. Comparison of 4DP-SMCs with SMCs proposed in other representative works [51].

Shape memory ceramics' composition for material universality	**Processing method for geometrical flexibility**	**Structural dimensions**	**Flexibility of shape memory capability**	**Mechanism of shape memory ceramics**
SiOC-based ceramics derived from elastic precursors (G. Liu *et al. Adv. Mater.* **2023**, 35, 2302108)	4D additive-subtractive manufacturing (2D/3D printing + laser engraving/cutting)	macroscale (over 4 cm)	original/reverse, global/local	heterogeneity in thermal expansion-shrinkage behaviour
$(Zr/Hf)O_2(YNb)O_4$ (H. Gu *et al. Nature* **2021**, 599, 416)	ceramic powder pressing	mesoscale (4 mm)	original, global	martensitic phase transformation
ZrO_2-based ceramics (A. Lai *et al. Science* **2013**, 341, 1505)	Ceramic powder pressing + focused ion beam	microscale (6 μm)	original, global	martensitic phase transformation

4. Conclusion

As technology continues to advance, improved precision and efficiency in ceramic 3D printing can be anticipated. Volume-by-volume printing and block-by-block printing may be the main directions of future research as they can enhance the efficiency of manufacturing ceramic materials [1] (**Fig. 21(a)**). With the development of interdisciplinary research, multi-material, multi-modulus, multi-scale, multi-system, multi-dimensional, and multi-function additive manufacturing [1] (**Fig. 21(b)**) for structural materials will provide multiple solutions for the material–structure–performance integrated additive manufacturing (MSPI-AM) [144] and intelligent manufacturing

[145, 146]. The impressive study in hierarchical design of 3D printed architectures puts forward opportunities in the superior property with challenges in the novel process [147]. The comprehensive understanding of distortion in additive manufacturing of structural materials would be inspiring for scientific research and industrial application [148]. 4D printing of EDCs, as an intelligent [149] and future [150] manufacturing technology, can offer potential for the application of high-temperature structural materials in aerospace, electronics, biomedical, and art domains, among other fields [51] (**Fig. 21(c)**). 4D-ASMC embodies the integration of Chinese traditional ceramic arts and modern advanced manufacturing technologies, and enables new solutions to the manufacturing of smart bionic structures connecting nature and technology [151]. 4DP-SMCs, as a new 4D printing shape memory materials, would play a significant role in developing functional materials [152]. The versatile morphing materials [153-155] and driving mechanism [156, 157] for 4D printing are inspiring researchers to devise solutions for specific ceramic manufacturing needs. New equipment, including advanced and high-end manufacturing equipment [158, 159], would be derived from and also promote the development of new material, new process, new function.

Fig. 21. Prospects for ceramic printing: (a) Development trend of ceramic printing techniques [1]; (b) Multiple perspectives of additive manufacturing for structural materials [1]; (c) Potential applications of ceramic 4D printing [51].

Declaration of competing interest

The authors declare that they have no known competing financial interests or personal relationships that could have appeared to influence the work reported in this paper.

CRediT authorship contribution statement

Xinya Lu: Investigation, Visualization, Writing – original draft, Writing – review & editing.

Guo Liu：Investigation, Visualization, Writing – original draft, Writing – review & editing.

Jian Lu：Conceptualization, Funding acquisition, Project administration, Supervision, Writing – review & editing.

Acknowledgements

This work was supported by Shenzhen-Hong Kong Science and Technology Innovation Cooperation Zone Shenzhen Park Project (Grant No. HZQB-KCZYB-2020030), Shenzhen Science and Technology Program (Grant No. JCYJ20220818101204010), Hong Kong Innovation and Technology Commission via the Hong Kong Branch of National Precious Metals Material Engineering Research Center; and the Research Grants Council of Hong Kong Special Administrative Region, China (Grant No. AoE/M-402/20). The authors thank the helpful discussions with Prof. Lei Zhang on the craft and art of ancient Chinese ceramics.

References

[1] Liu G, Zhang X, Chen X, et al. Additive manufacturing of structural materials. Materials Science and Engineering: R: Reports, 2021, 145: 100596.

[2] Chen Z, Li Z, Li J, et al. 3D printing of ceramics: A review. Journal of the European Ceramic Society, 2019, 39(4): 661-687.

[3] Lakhdar Y, Tuck C, Binner J, et al. Additive manufacturing of advanced ceramic materials. Progress in Materials Science, 2021, 116: 100736.

[4] Mueller B. Additive manufacturing technologies–Rapid prototyping to direct digital manufacturing. Assembly Automation, 2012, 32(2).

[5] Gibson I, Rosen D, Stucker B, et al. Additive manufacturing technologies: Material jetting. Springer 2021: 203-235.

[6] Dong H, Carr W W, Morris J F. An experimental study of drop-on-demand drop formation. Physics of Fluids, 2006, 18(7):072102.

[7] Ping B, Huang J, Meng F. Prediction model and compensation method for curing shrinkage of inkjet 3D printing parts. Journal of Manufacturing Processes, 2023, 101: 807-819.

[8] Shah M A, Lee D G, Lee B Y, et al. Classifications and applications of inkjet printing technology: A review. IEEE Access, 2021, 9: 140079-102.

[9] Chen Z, Ouyang J, Liang W, et al. Development and characterizations of novel aqueous-based LSCF suspensions for inkjet printing. Ceramics International, 2018, 44(11): 13381-13388.

[10] Qu P, Xiong D, Zhu Z, et al. Inkjet printing additively manufactured multilayer SOFCs using high quality ceramic inks for performance enhancement. Additive Manufacturing, 2021, 48: 102394.

[11] Wang X, Xiong D, Chen Z. Effective post-processing strategies of inkjet-printed ceramic cathodes for improved fuel cell performance. Ceramics International, 2023, 49(24): 40593-40600.

[12] Huang Z, Tang Y, Guo H, et al. 3D printing of ceramics and graphene circuits-on-ceramics by thermal bubble inkjet technology and high temperature sintering. Ceramics International, 2020, 46(8): 10096-10104.

[13] Zhang B, Pei X, Song P, et al. Porous bioceramics produced by inkjet 3D printing: Effect of printing ink formulation on the ceramic macro and micro porous architectures control. Composites Part B: Engineering, 2018, 155: 112-121.

[14] Zhang B, Sun H, Wu L, et al. 3D printing of calcium phosphate bioceramic with tailored biodegradation rate for skull bone tissue reconstruction. Bio-Design and Manufacturing, 2019, 2: 161-171.

[15] Liang C, Huang J, Wang J, et al. Three-dimensional inkjet printing and low temperature sintering of silica-based ceramics. Journal of the European Ceramic Society, 2023, 43(5): 2289-2294.

[16] Liang C, Huang J, Wang J, et al. Additive manufacturing of low-temperature co-fired ceramic substrates and surface conductors based on material jetting. Additive Manufacturing, 2023, 78: 103856.

[17] Zhong S, Shi Q, Deng Y, et al. High-performance zirconia ceramic additively manufactured via nanoparticle jetting. Ceramics International, 2022, 48(22): 33485-33498.

[18] Dimitrov D, Schreve K, De Beer N. Advances in three dimensional printing–state of the art and future perspectives. Rapid Prototyping Journal, 2006, 12(3): 136-147.

[19] Feng K, Hu S, Li L, et al. Preparation of low residual silicon content Si-SiC ceramics by binder jetting additive manufacturing and liquid silicon infiltration. Journal of the European Ceramic Society, 2023, 43(13): 5446-5457.

[20] Zhao W, Liu W, Wu J, et al. 316L-toughened porous Al_2O_3-based ceramic functionally graded materials using binder jetting. Ceramics International, 2023, 49(24): 39760-70.

[21] Huang S, Ye C, Zhao H, et al. Additive manufacturing of thin alumina ceramic cores using binder-jetting. Additive Manufacturing, 2019, 29: 100802.

[22] Yu T, Zhao Z, Li J. Effect of sintering temperature and sintering additives on the properties of alumina ceramics fabricated by binder jetting. Ceramics International, 2023, 49(6): 9948-9955.

[23] Zhao H, Ye C, Xiong S, et al. Fabricating an effective calcium zirconate layer over the calcia grains via

binder-jet 3D-printing for improving the properties of calcia ceramic cores. Additive Manufacturing, 2020, 32: 101025.

[24] Zhao H, Wang A, Li G, et al. Improving the properties of binder jetted ceramics via nanoparticle dispersion infiltration. Ceramics International, 2022, 48(22): 33580-33587.

[25] Zhao W, Liu W, Chang J, et al. Properties comparison of pure Al_2O_3 and doped Al_2O_3 ceramic cores fabricated by binder jetting additive manufacturing. Ceramics International, 2023, 49(24): 40336-10346.

[26] Saadi M, Maguire A, Pottackal N T, et al. Direct ink writing: A 3D printing technology for diverse materials. Advanced Materials, 2022, 34(28): 2108855.

[27] Tsang A C H, Zhang J, Hui K N, et al. Recent development and applications of advanced materials via direct ink writing. Advanced Materials Technologies, 2022, 7(7): 2101358.

[28] Yang Y, Cai D, Yang Z, et al. Rheology of organics-free aqueous ceramic suspensions for additive manufacturing of dense silicon nitride ceramics. Ceramics International, 2022, 48(21): 31941-51.

[29] Yang Y, Yang Z, He P, et al. Si_3N_4 ceramics with embedded microchannel structures fabricated by high-precision additive manufacturing based on computational fluid dynamics simulations. Additive Manufacturing, 2022, 60: 103271.

[30] Yang Y, Yang Z, Duan X, et al. Large-size Si_3N_4 ceramic fabricated by additive manufacturing using long-term stable hydrogel-based suspensions. Additive Manufacturing, 2023, 69: 103534.

[31] Zhang X, Huo W, Liu J, et al. 3D printing boehmite gel foams into lightweight porous ceramics with hierarchical pore structure. Journal of the European Ceramic Society, 2020, 40(3): 930-934.

[32] Zhang X, Zhang Y, Lu Y, et al. Hierarchically porous ceria with tunable pore structure from particle-stabilized foams. Journal of the European Ceramic Society, 2020, 40(12): 4366-4372.

[33] Wei L, Li J, Zhang S, et al. Fabrication of SiOC ceramic with cellular structure via UV-Assisted direct ink writing. Ceramics International, 2020, 46(3): 3637-3643.

[34] Wang X, Sun Y, Peng C, et al. Transitional suspensions containing thermosensitive dispersant for three-dimensional printing. ACS applied materials & interfaces, 2015, 7(47): 26131-26136.

[35] Yang L, Zeng X, Ditta A, et al. Preliminary 3D printing of large inclined-shaped alumina ceramic parts by direct ink writing. Journal of Advanced Ceramics, 2020, 9: 312-319.

[36] Chen H, Wang X, Xue F, et al. 3D printing of SiC ceramic: Direct ink writing with a solution of preceramic polymers. Journal of the European Ceramic Society, 2018, 38(16): 5294-5300.

[37] Pan Y, Zhu P, Wang R, et al. Direct ink writing of porous cordierite honeycomb ceramic. Ceramics International, 2019, 45(12): 15230-6.

[38] Lao D, Zhang Y, Chen R, et al. Novel ceramic supports for catalyst with hierarchical pore structures fabricated via additive manufacturing-direct ink writing. Journal of the European Ceramic Society, 2024.

[39] Huo C, Tian X, Chen C, et al. Hierarchically porous alumina catalyst carrier with biomimetic vein structure prepared by direct ink writing. Journal of the European Ceramic Society, 2021, 41(7): 4231-41.

[40] Zhong G, Vaezi M, Liu P, et al. Characterization approach on the extrusion process of bioceramics for the 3D printing of bone tissue engineering scaffolds. Ceramics International, 2017, 43(16): 13860-8.

[41] Wu L, Zhou C, Zhang B, et al. Construction of biomimetic natural wood hierarchical porous-structure bioceramic with micro/nanowhisker coating to modulate cellular behavior and osteoinductive activity. ACS Applied Materials & Interfaces, 2020, 12(43): 48395-407.

[42] Liu G, He Y, Liu P, et al. Development of bioimplants with 2D, 3D, and 4D additive manufacturing materials. Engineering, 2020, 6(11): 1232-43.

[43] Zhu Q, Dong X, Hu J, et al. High strength aligned SiC nanowire reinforced SiC porous ceramics fabricated by 3D printing and chemical vapor infiltration. Ceramics International, 2020, 46(5): 6978-83.

[44] Xiong H, Chen H, Zhao L, et al. SiCw/SiCp reinforced 3D-SiC ceramics using direct ink writing of polycarbosilane-based solution: Microstructure, composition and mechanical properties. Journal of the European Ceramic Society, 2019, 39(8): 2648-57.

[45] Ji H, Chen H, Zhang B, et al. Direct ink writing of aluminium oxynitride (AlON) transparent ceramics

from water-based slurries. Ceramics International, 2022, 48(6): 8118-24.
[46] Zhang G, Carloni D, Wu Y. 3D printing of transparent YAG ceramics using copolymer-assisted slurry. Ceramics International, 2020, 46(10): 17130-4.
[47] Li B, Xue Z, Jiang B, et al. 3D printing of infrared transparent ceramics via material extrusion. Additive Manufacturing, 2023, 61: 103364.
[48] Liu Q, Li Z, Li J, et al. Three dimensional BaTiO3 piezoelectric ceramics coated with TiO_2 nanoarray for high performance of piezo-photoelectric catalysis. Nano Energy, 2022, 98: 107267.
[49] Li Z, Li J, Luo H, et al. Direct ink writing of 3D piezoelectric ceramics with complex unsupported structures. Journal of the European Ceramic Society, 2022, 42(9): 3841-7.
[50] Liu G, Zhao Y, Wu G, et al. Origami and 4D printing of elastomer-derived ceramic structures. Science Advances, 2018, 4(8): eaat0641.
[51] Liu G, Zhang X, Lu X, et al. 4D additive–subtractive manufacturing of shape memory ceramics. Advanced Materials, 2023, 35(39): 2302108.
[52] Liu G, Lu X, Zhang X, et al. 3D/4D additive–subtractive manufacturing of heterogeneous ceramics. Journal of Materials Science & Technology, 2024, 201: 210-21.
[53] Tan X, Obaid R F, Smaisim G F, et al. Investigation of addition of calcium phosphate ceramic to multilayer scaffold for bone applications with improved mechanical properties: Fuzzy logic analysis. Ceramics International, 2023, 49(5): 8339-49.
[54] Niu F, Yang X, Li Y, et al. Fused deposition modeling of Si_3N_4 ceramics: A cost-effective 3D-printing route for dense and high performance non-oxide ceramic materials. Journal of the European Ceramic Society, 2022, 42(15): 7369-76.
[55] He Q, Jiang J, Yang X, et al. Additive manufacturing of dense zirconia ceramics by fused deposition modeling via screw extrusion. Journal of the European Ceramic Society, 2021, 41(1): 1033-40.
[56] Shen T, Xiong H, Li Z, et al. Fused deposition fabrication of high-quality zirconia ceramics using granular feedstock. Ceramics International, 2021, 47(24): 34352-60.
[57] Zhao L, Wang X, Xiong H, et al. Optimized preceramic polymer for 3D structured ceramics via fused deposition modeling. Journal of the European Ceramic Society, 2021, 41(10): 5066-74.
[58] Ma H, Feng C, Chang J, et al. 3D-printed bioceramic scaffolds: From bone tissue engineering to tumor therapy. Acta Biomaterialia, 2018, 79: 37-59.
[59] Zhang B, Wang L, Song P, et al. 3D printed bone tissue regenerative PLA/HA scaffolds with comprehensive performance optimizations. Materials & Design, 2021, 201: 109490.
[60] Wang L, Pang Y, Tang Y, et al. A biomimetic piezoelectric scaffold with sustained Mg^{2+} release promotes neurogenic and angiogenic differentiation for enhanced bone regeneration. Bioactive Materials, 2023, 25: 399-414.
[61] Noordin N N F N M, Ahmad N, Jaafar M, et al. A review of bioceramics scaffolds for bone defects in different types of animal models: HA and β-TCP. Biomedical Physics & Engineering Express, 2022, 8(5): 052002.
[62] Chen S, Sun D, Wang C, et al. Alumina-based ceramic mold with integral core and shell for hollow turbine blades fabricated by laser powder bed fusion. Additive Manufacturing, 2022, 58: 103046.
[63] Zhang J, Wu J M, Liu H, et al. Microstructure and properties of silica-based ceramic cores by laser powder bed fusion combined with vacuum infiltration. Journal of Materials Science & Technology, 2023, 157: 71-9.
[64] Huo C, Tian X, Nan Y, et al. Hierarchically porous alumina ceramic catalyst carrier prepared by powder bed fusion. Journal of the European Ceramic Society, 2020, 40(12): 4253-64.
[65] Huo C, Tian X, Nan Y, et al. Regulation mechanism of the specific surface area of alumina ceramic carriers with hierarchical porosity fabricated by powder bed fusion. Ceramics International, 2021, 47(21): 30954-62.
[66] Liu Z, Song K, Gao B, et al. Microstructure and mechanical properties of Al_2O_3/ZrO_2 directionally solidified eutectic ceramic prepared by laser 3D printing. Journal of Materials Science & Technology, 2016, 32(4): 320-5.
[67] Shen Z, Su H, Yu M, et al. Large-size complex-structure ternary eutectic ceramic fabricated using laser powder bed fusion assisted with finite element analysis. Additive Manufacturing, 2023, 72:

103627.
[68] Wu S, Yang L, Wang C, et al. Si/SiC ceramic lattices with a triply periodic minimal surface structure prepared by laser powder bed fusion. Additive Manufacturing, 2022, 56: 102910.
[69] Zhu W, Fu H, Xu Z, et al. Fabrication and characterization of carbon fiber reinforced SiC ceramic matrix composites based on 3D printing technology. Journal of the European Ceramic Society, 2018, 38(14): 4604-4613.
[70] Liu K, Wu T, Bourell D L, et al. Laser additive manufacturing and homogeneous densification of complicated shape SiC ceramic parts. Ceramics International, 2018, 44(17): 21067-21075.
[71] Wu Z, Sun D, Shi C, et al. Moisture-thermal stable, superhydrophilic alumina-based ceramics fabricated by a selective laser sintering 3D printing strategy for solar steam generation. Advanced Functional Materials, 2023, 33(45): 2304897.
[72] Chen A N, Li M, Xu J, et al. High-porosity mullite ceramic foams prepared by selective laser sintering using fly ash hollow spheres as raw materials. Journal of the European Ceramic Society, 2018, 38(13): 4553-9.
[73] Liu S S, Li M, Wu J M, et al. Preparation of high-porosity Al_2O_3 ceramic foams via selective laser sintering of Al_2O_3 poly-hollow microspheres. Ceramics International, 2020, 46(4): 4240-4247.
[74] Liu H, Su H, Shen Z, et al. One-step additive manufacturing and microstructure evolution of melt-grown Al_2O_3/$GdAlO_3$/ZrO_2 eutectic ceramics by laser directed energy deposition. Journal of the European Ceramic Society, 2021, 41(6): 3547-3558.
[75] Yan S, Huang Y, Zhao D, et al. 3D printing of nano-scale Al_2O_3-ZrO_2 eutectic ceramic: Principle analysis and process optimization of pores. Additive Manufacturing, 2019, 28: 120-126.
[76] Wu D, Yu X, Zhao Z, et al. One-step additive manufacturing of TiCp reinforced Al_2O_3–ZrO_2 eutectic ceramics composites by laser directed energy deposition. Ceramics International, 2023, 49(8): 12758-12771.
[77] Wu D, Shi J, Niu F, et al. Direct additive manufacturing of melt growth Al_2O_3-ZrO_2 functionally graded ceramics by laser directed energy deposition. Journal of the European Ceramic Society, 2022, 42(6): 2957-2973.
[78] Liu H, Su H, Shen Z, et al. Preparation of large-size Al_2O_3/$GdAlO_3$/ZrO_2 ternary eutectic ceramic rod by laser directed energy deposition and its microstructure homogenization mechanism. Journal of Materials Science & Technology, 2021, 85: 218-223.
[79] Liu H, Su H, Shen Z, et al. Insights into high thermal stability of laser additively manufactured Al_2O_3/$GdAlO_3$/ZrO_2 eutectic ceramics under high temperatures. Additive Manufacturing, 2021, 48: 102425.
[80] Li X, Su H, Dong D, et al. Enhanced comprehensive properties of stereolithography 3D printed alumina ceramic cores with high porosities by a powder gradation design. Journal of Materials Science & Technology, 2022, 131: 264-275.
[81] Dong D, Su H, Li X, et al. Microstructures and mechanical properties of biphasic calcium phosphate bioceramics fabricated by SLA 3D printing. Journal of Manufacturing Processes, 2022, 81: 433-43.
[82] Zhang W, Lian Q, Li D, et al. The effect of interface microstructure on interfacial shear strength for osteochondral scaffolds based on biomimetic design and 3D printing. Materials Science and Engineering: C, 2015, 46: 10-15.
[83] Zhang K, He R, Ding G, et al. Effects of fine grains and sintering additives on stereolithography additive manufactured Al_2O_3 ceramic. Ceramics International, 2021, 47(2): 2303-2310.
[84] He R, Ding G, Zhang K, et al. Fabrication of SiC ceramic architectures using stereolithography combined with precursor infiltration and pyrolysis. Ceramics International, 2019, 45(11): 14006-14014.
[85] Chen R, Lian Q, He X, et al. A stereolithographic diamond-mixed resin slurry for complex SiC ceramic structures. Journal of the European Ceramic Society, 2021, 41(7): 3991-3999.
[86] Xiao C, Zheng K, Chen S, et al. Additive manufacturing of high solid content lunar regolith simulant paste based on vat photopolymerization and the effect of water addition on paste retention properties. Additive Manufacturing, 2023, 71: 103607.
[87] Qian C, Hu K, Li J, et al. The effect of light scattering in stereolithography ceramic manufacturing.

Journal of the European Ceramic Society, 2021, 41(14): 7141-7154.
[88] Wang K, Liu R, Bao C. SiC paste with high curing thickness for stereolithography. Ceramics International, 2022, 48(19): 28692-28703.
[89] Li S, Bao C, Ma H, et al. Fabrication and properties of diatomite ceramics with hierarchical pores based on direct stereolithography. Ceramics International, 2022, 48(5): 6266-6276.
[90] Zhang L, Feih S, Daynes S, et al. Pseudo-ductile fracture of 3D printed alumina triply periodic minimal surface structures. Journal of the European Ceramic Society, 2020, 40(2): 408-416.
[91] Wu H, Liu W, He R, et al. Fabrication of dense zirconia-toughened alumina ceramics through a stereolithography-based additive manufacturing. Ceramics International, 2017, 43(1): 968-972.
[92] Zhao G, Hu K, Feng Q, et al. Creep mechanism of zircon-added silica ceramic cores formed by stereolithography. Ceramics International, 2021, 47(12): 17719-17725.
[93] Dong W, Ma H, Liu R, et al. Fabrication by stereolithography of fiber-reinforced fused silica composites with reduced crack and improved mechanical properties. Ceramics International, 2021, 47(17): 24121-24129.
[94] Wang H, Liu L Y, Ye P, et al. 3D printing of transparent spinel ceramics with transmittance approaching the theoretical limit. Advanced Materials, 2021, 33(15): 2007072.
[95] Chen Y, Bao X, Wong C M, et al. PZT ceramics fabricated based on stereolithography for an ultrasound transducer array application. Ceramics International, 2018, 44(18): 22725-30.
[96] Zhang K, Wang K, Chen J, et al. Design and additive manufacturing of 3D-architected ceramic metamaterials with programmable thermal expansion. Additive Manufacturing, 2021, 47: 102338.
[97] Li Z, Jia Y, Duan K, et al. One-photon three-dimensional printed fused silica glass with sub-micron features. Nature Communications, 2024, 15(1): 2689.
[98] Kumar H, Kim K. Stereolithography 3D bioprinting. 3D Bioprinting: Principles and Protocols, 2020: 93-108.
[99] Li Z, Chen Z, Liu J, et al. Additive manufacturing of lightweight and high-strength polymer-derived SiOC ceramics. Virtual and Physical Prototyping, 2020, 15(2): 163-77.
[100] Fu Y, Xu G, Chen Z, et al. Multiple metals doped polymer-derived SiOC ceramics for 3D printing. Ceramics International, 2018, 44(10): 11030-8.
[101] Zhang L, Zeng Y, Yao H, et al. Fabrication and characterization of ZrO_2 (3Y)/Al_2O_3 micro-ceramic gears with high performance by vat photopolymerization 3D printing. Ceramics International, 2024, 50(3): 5187-97.
[102] Zhang X, Meng Q, Zhang K, et al. 3D-printed bioinspired Al_2O_3/polyurea dual-phase architecture with high robustness, energy absorption, and cyclic life. Chemical Engineering Journal, 2023, 463: 142378.
[103] Zhao D, Su H, Hu K, et al. Formation mechanism and controlling strategy of lamellar structure in 3D printed alumina ceramics by digital light processing. Additive Manufacturing, 2022, 52: 102650.
[104] Duan W, Li S, Wang G, et al. Thermal conductivities and mechanical properties of AlN ceramics fabricated by three dimensional printing. Journal of the European Ceramic Society, 2020, 40(10): 3535-40.
[105] Chen Z, Li J, Liu C, et al. Preparation of high solid loading and low viscosity ceramic slurries for photopolymerization-based 3D printing. Ceramics International, 2019, 45(9): 11549-57.
[106] Guo J, Zeng Y, Li P, et al. Fine lattice structural titanium dioxide ceramic produced by DLP 3D printing. Ceramics International, 2019, 45(17): 23007-12.
[107] Sun j, Chen x, Wade-Zhu J, et al. A comprehensive study of dense zirconia components fabricated by additive manufacturing. Additive Manufacturing, 2021, 43: 101994.
[108] Jiao C, Xie D, He Z, et al. Additive manufacturing of bio-inspired ceramic bone scaffolds: Structural design, mechanical properties and biocompatibility. Materials & Design, 2022, 217: 110610.
[109] Liu Z, Liang H, Shi T, et al. Additive manufacturing of hydroxyapatite bone scaffolds via digital light processing and in vitro compatibility. Ceramics International, 2019, 45(8): 11079-86.
[110] Zhang H, Jiao C, He Z, et al. Fabrication and properties of 3D printed zirconia scaffold coated with calcium silicate/hydroxyapatite. Ceramics International, 2021, 47(19): 27032-41.
[111] He Z, Jiao C, Zhang H, et al. Fabrication of a zirconia/calcium silicate composite scaffold based on

digital light processing. Ceramics International, 2022, 48(18): 25923-25932.
[112] Liu S, Chen J, Chen T, et al. Fabrication of trabecular-like beta-tricalcium phosphate biomimetic scaffolds for bone tissue engineering. Ceramics International, 2021, 47(9): 13187-13198.
[113] Liu S, Mo L, Bi G, et al. DLP 3D printing porous β-tricalcium phosphate scaffold by the use of acrylate/ceramic composite slurry. Ceramics International, 2021, 47(15): 21108-21116.
[114] Guo J, Zhang X, Yan J, et al. Digital light processing bio-scaffolds of hydroxyapatite ceramic foams with multi-level pores using Pickering emulsions as the feedstock. Journal of the European Ceramic Society, 2024, 44(6): 4272-4284.
[115] Wang J, Tang Y, Cao Q, et al. Fabrication and biological evaluation of 3D-printed calcium phosphate ceramic scaffolds with distinct macroporous geometries through digital light processing technology. Regenerative Biomaterials, 2022, 9: rbac005.
[116] Qi S, Lian Q, Chen Y, et al. Talcum powder coated polydimethylsiloxane (PDMS) film flexible large-deformation separation system and stable forming process in bottom-up ceramic vat photopolymerization. Additive Manufacturing, 2024, 83: 104083.
[117] Song C, Chen Y, Liu Z, et al. Rapid and high-accuracy forming of ceramic parts by DLP technology based on optimization of shear stress. Journal of the European Ceramic Society, 2024, 44(3): 1748-1760.
[118] Hu K, Zhao P, Li J, et al. High-resolution multiceramic additive manufacturing based on digital light processing. Additive Manufacturing, 2022, 54: 102732.
[119] Cheng J, Wang R, Sun Z, et al. Centrifugal multimaterial 3D printing of multifunctional heterogeneous objects. Nature Communications, 2022, 13(1): 7931.
[120] Li Q, Meng X, Zhang X, et al. Enhanced 3D printed Al_2O_3 core via in-situ mullite. Additive Manufacturing, 2022, 55: 102826.
[121] Li H, Liu Y, Liu Y, et al. Influence of debinding holding time on mechanical properties of 3D-printed alumina ceramic cores. Ceramics International, 2021, 47(4): 4884-4894.
[122] Lin L, Wu H, Ni P, et al. Additive manufacturing of complex-shaped and high-performance aluminum nitride-based components for thermal management. Additive Manufacturing, 2022, 52: 102671.
[123] Sheng P, Nie G, Li Y, et al. Enhanced curing behavior, mechanical and thermal properties of 3D printed aluminum nitride ceramics using a powder coating strategy. Additive Manufacturing, 2023, 74: 103732.
[124] Hu B, Zou W, Wu W, et al. Enhanced mechanical and sintering properties of MgO-TiO_2 ceramic composite via digital light processing. Journal of the European Ceramic Society, 2022, 42(4): 1694-1702.
[125] Li B, Wang S, Chen J, et al. 3D Printing of LuAG: Ce transparent ceramics for laser-driven lighting. Ceramics International, 2023, 49(23): 38708-38116.
[126] Chen R, Duan W, Wang G, et al. Preparation of broadband transparent Si_3N_4-SiO_2 ceramics by digital light processing (DLP) 3D printing technology. Journal of the European Ceramic Society, 2021, 41(11): 5495-504.
[127] Jiang Z, Cheng L, Zeng Y, et al. 3D printing of porous scaffolds $BaTiO_3$ piezoelectric ceramics and regulation of their mechanical and electrical properties. Ceramics International, 2022, 48(5): 6477-6487.
[128] Zhou R, Wang Y, Liu Z, et al. Digital light processing 3D-printed ceramic metamaterials for electromagnetic wave absorption. Nano-Micro Letters, 2022, 14(1): 122.
[129] Yao L, Yang W, Zhou S, et al. Top-down parametrization-design of orientation-reinforced SiOC-based perfect metamaterial microwave absorber with wide-temperature adaptability. Acta Materialia, 2023, 249: 118803.
[130] Xing R, Xu G, Qu N, et al. 3D printing of liquid-metal-in-ceramic metamaterials for high-efficient microwave absorption. Advanced Functional Materials, 2023: 2307499.
[131] Xu G, Hu K, Zhou R, et al. DLP–printable hyperbranched polyborosilazane for microwave absorbing SiBCN (O) ceramic metastructure. Ceramics International, 2024, 50(1): 781-790.
[132] Zhou Q, Liu H, Gu Y, et al. 3D printed PyC/Al_2O_3 ceramic metamaterials with different micro-channels for tunable microwave absorption. Journal of the European Ceramic Society, 2024, 44(1): 270-276.

[133] Liu H, Zhang Y, Liu X, et al. Additive manufacturing of nanocellulose/polyborosilazane derived CNFs-SiBCN ceramic metamaterials for ultra-broadband electromagnetic absorption. Chemical Engineering Journal, 2022, 433: 133743.

[134] Liu X, Liu H, Wu H, et al. Structural electromagnetic absorber based on MoS_2/PyC-Al_2O_3 ceramic metamaterials. Small, 2023, 19(33): 2300664.

[135] Zhang G, Chen H, Yang S, et al. Frozen slurry-based laminated object manufacturing to fabricate porous ceramic with oriented lamellar structure. Journal of the European Ceramic Society, 2018, 38(11): 4014-4019.

[136] Zhang G, Guo J, Chen H, et al. Organic mesh template-based laminated object manufacturing to fabricate ceramics with regular micron scaled pore structures. Journal of the European Ceramic Society, 2021, 41(4): 2790-2795.

[137] Whyte D J, Doeven E H, Sutti A, et al. Volumetric additive manufacturing: A new frontier in layer-less 3D printing. Additive Manufacturing, 2024: 104094.

[138] Madrid-Wolff J, Toombs J, Rizzo R, et al. A review of materials used in tomographic volumetric additive manufacturing. MRS Communications, 2023, 13(5): 764-785.

[139] Toombs J T, Luitz M, Cook C C, et al. Volumetric additive manufacturing of silica glass with microscale computed axial lithography. Science, 2022, 376(6590): 308-312.

[140] Warnke P, Cuhls K, Schmoch U, et al. 100 radical innovation breakthroughs for the future. European Commission, 2019.

[141] Fan J F, Liu G, Zhuo X S, et al. In-situ reaction synthesis Al_2O_3 overlay modified 7YSZ TBC for NaCl hot corrosion. Ceramics International, 2021, 47(16): 22404-22415.

[142] Cawley J D. Solid freeform fabrication of ceramics. Current Opinion in Solid State and Materials Science, 1999, 4(5): 483-489.

[143] Hagen G, Kopp T, Ziesche S, et al. Combined 3D micro structuring of ceramic green tape using punching, embossing and laser processing. Additional Papers and Presentations, 2012, 2012(CICMT): 000341-7.

[144] Gu D, Shi X, Poprawe R, et al. Material-structure-performance integrated laser-metal additive manufacturing. Science, 2021, 372(6545): eabg1487.

[145] Tian X, Wu L, Gu D, et al. Roadmap for additive manufacturing: Toward intellectualization and industrialization. Chinese Journal of Mechanical Engineering: Additive Manufacturing Frontiers, 2022, 1(1): 100014.

[146] Sun B, Shu D,Fu H, et al. Intelligent manufacturing for high-end new materials: Opportunities and directions. Strategic Study of Chinese Academy of Engineering, 2023, 25(3): 152-160.

[147] Zhang L, Hu Z, Wang M Y, et al. Hierarchical sheet triply periodic minimal surface lattices: design, geometric and mechanical performance. Materials & Design, 2021, 209: 109931.

[148] Xie D, Lv F, Liang H, et al. Towards a comprehensive understanding of distortion in additive manufacturing based on assumption of constraining force. Virtual and Physical Prototyping, 2021, 16(sup1): S85-S97.

[149] Shi Y, Wu H, Yan C, et al. Four-dimensional printing——the additive manufacturing technology of intelligent components. Journal of Mechanical Engineering, 2020, 56(15): 1-25.

[150] Tan C, Zou J, Fu Z. 4D printing for future manufacturing. Science China Materials, 2023, 66(11): 4517-8.

[151] Li X, Zhang S, Jiang P, et al. Smart bionic structures: Connecting nature and technology through additive manufacturing. Additive Manufacturing Frontiers, 2024: 200137.

[152] Luo L, Zhang F, Wang L, et al. Recent advances in shape memory polymers: Multifunctional materials, multiscale structures, and applications. Advanced Functional Materials, 2023: 2312036.

[153] Wang Q, Tian X, Zhang D, et al. Programmable spatial deformation by controllable off-center freestanding 4D printing of continuous fiber reinforced liquid crystal elastomer composites. Nature Communications, 2023, 14(1): 3869.

[154] Wu W, Zhou Y, Liu Q, et al. Metallic 4D Printing of Laser Stimulation. Advanced Science, 2023, 10(12): 2206486.

[155] Ou J, Huang M, Wu Y, et al. Additive manufacturing of flexible polymer-derived ceramic matrix

composites. Virtual and Physical Prototyping, 2023, 18(1): e2150230.
[156] Wang R, Yuan C, Cheng J, et al. Direct 4D printing of ceramics driven by hydrogel dehydration. Nature Communications, 2024, 15(1): 758.
[157] Li G, Yang S, Wu W, et al. Biomimetic 4D printing catapult: From biological prototype to practical implementation. Advanced Functional Materials, 2023, 33(32): 2301286.
[158] Wang L, Lu B. Development of additive manufacturing technology and industry in China. Strategic Study of Chinese Academy of Engineering, 2022, 24(4): 202-11.
[159] Shan Z, Song W, Fan C, et al. Development strategy for precision manufacturing of composite components facing 2035. Strategic Study of Chinese Academy of Engineering, 2023, 25(1): 113–20

The authors declare no conflict of interest.